

Taylor & Francis
Taylor & Francis Group

Journal of Biomolecular Structure and Dynamics

ISSN: (Print) (Online) Journal homepage: https://www.tandfonline.com/loi/tbsd20

Carbazole derivatives as promising competitive and allosteric inhibitors of human serotonin transporter: computational pharmacology

Yusuf Oloruntoyin Ayipo, Iqrar Ahmad, Chien Fung Chong, Nurul Amira Zainurin, Sani Yahaya Najib, Harun Patel & Mohd Nizam Mordi

To cite this article: Yusuf Oloruntoyin Ayipo, Iqrar Ahmad, Chien Fung Chong, Nurul Amira Zainurin, Sani Yahaya Najib, Harun Patel & Mohd Nizam Mordi (2023): Carbazole derivatives as promising competitive and allosteric inhibitors of human serotonin transporter: computational pharmacology, Journal of Biomolecular Structure and Dynamics, DOI: 10.1080/07391102.2023.2198016

To link to this article: https://doi.org/10.1080/07391102.2023.2198016

View supplementary material

Published online: 06 Apr 2023.

Submit your article to this journal

View related articles

View Crossmark data

Full Terms & Conditions of access and use can be found at
https://www.tandfonline.com/action/journalInformation?journalCode=tbsd20

JOURNAL OF BIOMOLECULAR STRUCTURE AND DYNAMICS
https://doi.org/10.1080/07391102.2023.2198016

Taylor & Francis
Taylor & Francis Group

Check for updates

Carbazole derivatives as promising competitive and allosteric inhibitors of human serotonin transporter: computational pharmacology

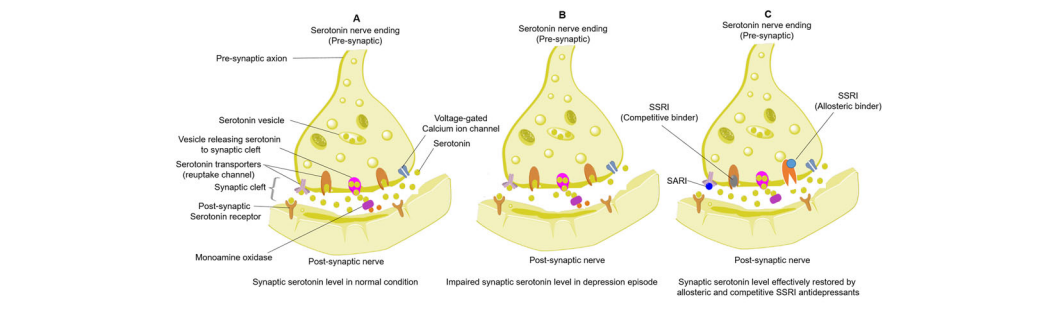
Yusuf Oloruntoyin Ayipo[a,b], Iqrar Ahmad[c,d], Chien Fung Chong[a,e], Nurul Amira Zainurin[f], Sani Yahaya Najib[a,g], Harun Patel[d] and Mohd Nizam Mordi[a]

[a]Centre for Drug Research, Universiti Sains Malaysia, USM, Pulau Pinang, Malaysia; [b]Department of Chemistry and Industrial Chemistry, Kwara State University, Ilorin, Nigeria; [c]Department of Pharmaceutical Chemistry, Prof Ravindra Nikam College of Pharmacy, Dhule, Maharashtra, India; [d]Department of Pharmaceutical Chemistry, R C Patel Institute of Pharmaceutical Education and Research, Shirpur, Maharashtra, India; [e]Department of Allied Health Sciences, Universiti Tunku Abdul Rahman, Kampar, Perak, Malaysia; [f]Faculty of Agro-Based Industry, Universiti Malaysia Kelantan, Jeli, Kelantan, Malaysia; [g]Department of Pharmaceutical and Medicinal Chemistry, Bayero University, Kano, Nigeria

Communicated by Ramaswamy H. Sarma

ABSTRACT

The human serotonin transporters (hSERTs) are neurotransmitter sodium symporters of the aminergic G protein-coupled receptors, regulating the synaptic serotonin and neuropharmacological processes related to neuropsychiatric disorders, notably, depression. Selective serotonin reuptake inhibitors (SSRIs) such as fluoxetine and (S)-citalopram are competitive inhibitors of hSERTs and are commonly the first-line medications for major depressive disorder (MDD). However, treatment-resistance and unpleasant aftereffects constitute their clinical drawbacks. Interestingly, vilazodone emerged with polypharmacological (competitive and allosteric) inhibitions on hSERTs, amenable to improved efficacy. However, its application usually warrants adjuvant/combination therapy, another subject of critical adverse events. Thus, the discovery of alternatives with polypharmacological potentials (one-drug-multiple-target) and improved safety remains essential. In this study, carbazole analogues from chemical libraries were explored using docking and molecular dynamics (MD) simulation. Selectively, two IBScreen ligands, **STOCK3S-30866** and **STOCK1N-37454** predictively bound to the active pockets and expanded boundaries (extracellular vestibules) of the hSERTs more potently than vilazodone and *(S)*-citalopram. For instance, the two ligands showed docking scores of −9.52 and −9.59 kcal/mol and MM-GBSA scores of −92.96 and −65.66 kcal/mol respectively compared to vilazodone's respective scores of −7.828 and −59.27 against the central active site of the hSERT (PDB 7LWD). Similarly, the two ligands also docked to the allosteric pocket (PDB 5I73) with scores of −8.15 and −8.40 kcal/mol and MM-GBSA of −96.14 and −68.46 kcal/mol whereas *(S)*-citalopram has −6.90 and −69.39 kcal/mol respectively. The ligands also conferred conformational stability on the receptors during 100 ns MD simulations and displayed interesting ADMET profiles, representing promising hSERT modulators for MDD upon experimental validation.



ARTICLE HISTORY
Received 4 October 2022
Accepted 25 March 2023

KEYWORDS
Major depressive disorder; serotonergic pathways; human serotonin transporter; molecular dynamics; carbazole alkaloids; computational pharmacology

Introduction

Depression is a complex, debilitating, heterogeneous, psychiatric disorder, affecting around 350 million people globally according to the World Health Organization (WHO) (Shadrina et al., 2018). Its paradigm usually associates several comorbidities, constituting risk factors from mild to deadly, including anxiety, mood disorder, bipolar disorders, treatment-resistance and suicidal ideation which particularly claims around 800,000 lives yearly. As a mental disorder, the burdens of major depressive disorder (MDD) spread across all categories of economies. It is more pronounced in

CONTACT Yusuf Oloruntoyin Ayipo yusuf.ayipo@kwasu.edu.ng Centre for Drug Research, Universiti Sains Malaysia, USM, Pulau Pinang, 11800, Malaysia
Supplemental data for this article can be accessed online at https://doi.org/10.1080/07391102.2023.2198016.
© 2023 Informa UK Limited, trading as Taylor & Francis Group

developed countries compared to their low- and middle-income counterparts. For instance, as of the year 2020, the direct annual capital burden of MDD in the US was estimated between $29–40 billion aside from indirect impacts on socio-economic lives (Ramadan & Mansour, 2020). The pathogenesis of depression is strongly implicated as both biological and psychological, with common symptoms such as apathy, depressive mood, impaired thinking, fatigue, and loss of concentration (de Sousa et al., 2006). A person is appropriately diagnosed with depression if five out of the nine key indicators manifest for most of the day continuously for a minimum of two weeks. The indicators include depressive mood, fatigue, loss of interest/pleasure, psychomotor agitation/retardation, drastic weight/appetite alteration, insomnia/hypersomnia, reduced thinking/cognitive ability, feeling worthless and suicidal ideation (ADAA, 2021; Brigitta, 2002; Vann, 2021). Being multifactorial, the involvement of several biomolecular carriers of neurotransmitters significantly contributes to the complex aetiology, pathophysiology and pharmacotherapy of the disease. These include the receptors for monoamine neurotransmitters including serotonin (5-HT), dopamine (DA) and norepinephrine (NA) (Chilmonczyk et al., 2017).

Serotonergic signalling is strongly implicated in some prominent psychiatric disorders including anxiety, schizophrenia and depression (Wray & Rasenick, 2019). Serotonin is vastly distributed across the central and peripheral nervous systems, coordinating important functions of the brain, cardiovascular, gastrointestinal and immune systems. In the central nervous system (CNS), it is localised near the 5-HT-releasing terminals and at the varicosities of the serotonergic neurons. As such, the serotonergic system significantly modulates various actions including mood, food intake, memory, sleep, perception and sexual behaviours (Y. Peng et al., 2018; Rudnick, 2007). Serotonin receptors are members of the cell surface and aminergic G protein-coupled receptors (GPCR) which are involved in serotonin-inclined physiological and psychophysiological activities within biological systems. The human serotonin transporters (hSERTs) are members of the neurotransmitter sodium symporter (NSS) class of the GPCR. They regulate the concentration of synaptic 5-HT and neuropharmacological processes related to mental disorders, relevantly contributing significantly to the pathogenesis, prophylaxis and treatment of depression (Immadisetty, 2015; Y. Peng et al., 2018). According to the serotonergic hypothesis, the diminished level of synaptic serotonin constitutes a major causal route in the pathophysiology of depression. This is inclusively induced by the SERTs through the reuptake of 5-HT in the synapses back to the pre-synaptic serotonergic neuron. As such, mechanistic inhibition of SERT modulates the synaptic 5-HT level, leading to downstream molecular and cellular adaptations, and inducing antidepressant pharmacology. These are the mechanisms of therapeutic actions of selective serotonin reuptake inhibitors (SSRIs) and serotonin antagonists and reuptake inhibitors (SARIs) among other antidepressants. Almost all current SSRIs exhibit competitive inhibitory interactions with hSERTs (Cowen & Browning, 2015; Rudnick, 2007; Wray & Rasenick, 2019). Recent studies have also shown that targeting the modulation of both central and allosteric sites of SERTs and other NSSs by neuroactive ligands as therapeutic pathways for MDD currently attracting scientific interest. Ligand binding competitively to the active pockets inhibits the reuptake of the synaptic 5-HT while the allosteric binding distorts the protein conformation including the active site, thereby mitigating the 5-HT reuptake. Both ways regulate the 5-HT level, a pharmacological pathway for managing depression (Figure 1) (Navratna et al., 2018; Plenge et al., 2020, 2021).

Selective serotonin reuptake inhibitors are the most commonly prescribed first-line antidepressants in clinical situations of MDD, mostly expressing mechanistic competitive inhibition on SERTs. Notably, escitalopram, fluoxetine, paroxetine, sertraline and vilazodone, each with characteristic medicinal challenges, efficacious challenges and side effects. For instance, the most commonly applied SSRI, fluoxetine is renowned for adverse effects such as nausea, insomnia, anxiety, sexual dysfunction, diarrhoea, hair loss, drowsiness and nervousness (Brody, 2018; Holshoe, 2016; Plenge et al., 2021). Moreover, SSRIs generally show delayed action and therapeutic failure in not less than 30% of patients with MDD. As such, their prescription usually involves adjuvants (polypharmacy), commonly with SARIs and sometimes nutritional supplements for improved efficacy and effective management of adverse syndromes (Ayipo et al., 2022; Moreira et al., 2022). However, the susceptibility of such required polypharmacy to additive adverse effects and severe drug-drug interactions with multiple medications poses another major challenge (Lexow et al., 2021; Sheikh-Taha & Asmar, 2021). To overcome this, interactions of an active ligand with multiple targets through network pharmacology (one-drug-multiple-targets) portray a plausible alternative for exploration.

Network pharmacology represents modern methods of elucidating diverse mechanisms of drug actions (S. I. Berger & Iyengar, 2009). Such techniques reportedly enhance the safety and therapeutic effects of drugs against diseases with complex heterogeneous aetiology including schizophrenia and depression (Y. Peng, McCorvy, et al., 2018; Si & Wang, 2014). Targeting the hSERTs, ligands binding to the antagonist-bound inactive conformation of the SERT tend to exhibit antagonistic inhibition competitively, as antidepressant expressions (Yuen et al., 2020). The SSRIs including *(S)*-citalopram and clomipramine usually bind competitively to the active site S1 of the SERT with high affinity while those with allosteric components display non-competitive inhibition. Moreover, the non-competitive inhibitors of SERTs are hypothesized to show more desirable therapeutic antidepressant effects, as demonstrated by vilazodone (Plenge et al., 2020; Sahli et al., 2016; Smithson & Mitchell, 2019). A recent study by Plenge *et al*. favoured vilazodone as an effective allosteric inhibitor of 5-HT uptake on hSERT (PDB 7LWD). Progressively, ligands with high affinities for site S2 of the SERT tend to inhibit the 5-HT transport through combined competitive and non-competitive inhibitory mechanisms. They hypothetically bind to both allosteric and central active sites thereby enhancing synergistic network pharmacology amenable to overcoming treatment resistance, loss of efficacy and undesired side effects (S. I. Berger & Iyengar, 2009; Plenge et al., 2021). An example is ((S)-1-(4-Fluorophenyl)-1-(3-(4-(2-oxo-1,2-dihydroquinolin-7-yl)piperidin-1-yl)propyl)-1,3-

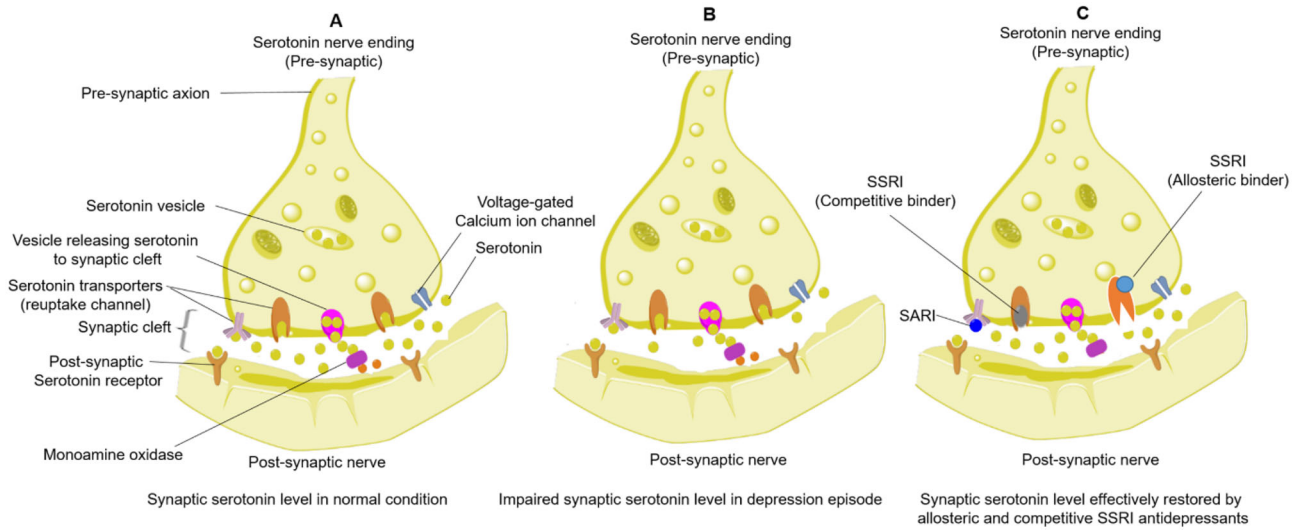


Figure 1. Pathomechanisms of depression through serotonin impairment and restoration effects of SSRI antidepressants through competitive and allosteric binding to the SERTs.

dihydroisobenzofuran-5-carboxamide) (Lu AF60097), recently reported with strong inhibition on both central active site and allosteric pockets of SERT (PDB 7LWD) (Plenge et al., 2021). Again, *(S)*-citalopram has also been reported to additionally bind to the allosteric pocket of the hSERT (PDB 5I73), thereby sterically locking and preventing the ligand unbinding from the active site. These synergistic monoligand-based polypharmacology demonstrate effective pathways for regulating 5-HT levels in depressive episode (Coleman et al., 2016; Plenge et al., 2020). Although, *(S)*-citalopram is recognized with a lower affinity for the extracellular vestibule allosteric pocket compared to paroxetine. However, the latter is notorious for the CYP2D6-mediated drug-drug interactions (Deodhar et al., 2020). These make the further probes for better neuroactive multi-mechanistic, competitive and allosteric SERT ligands remain attractive through the interactions with the aforementioned structures.

Carbazole is an N-containing tricyclic alkaloid, abundant in natural products with good synthetic accessibility. As a heterocycle, its molecular skeleton consists of a 5-membered pyrrolic ring fused to a benzene ring on each side. The structural organisation of its pharmacophoric sites including the fused aromatic rings favours interactions with various biological targets, as such, supports its large spectrum of biological and therapeutic applications. Several drugs and active prodrugs with carbazole scaffold have been designed (Hegden et al., 2020). These include aminopropyl carbazole P7C3, P7C3-A20 and their derivatives which actively protected neurons *in vivo* hippocampus of nonhuman primates. Their interactions with various neurological targets support pro-neurogenic and neuroprotective efficacy against several complex neurodegenerative diseases such as Alzheimer's and Parkinson's diseases where effective therapy remains challenging (Bauman et al., 2018; Hegden et al., 2020; Wang et al., 2014). Other labelled carbazole-based drugs include the α- and β-adrenergic receptor blockers such as carvedilol for treating high blood pressure and heart failure (Alapi & Fischer, 2006). Also, frovatriptan for migraine (Allais & Benedetto, 2016), NMP-7, a non-selective agonist of CB1 and CB2 cannabinoid receptors as well as a T-type calcium channel blocker analgesic belonging to the alkaloid analogues (N. D. Berger et al., 2014). In addition, carprofen, a non-steroidal anti-inflammatory drug (Huskisson, 1982), pirlindole for treating depression and fibromyalgia syndrome (Branco et al., 2011) and ciclindole/flucindole, antipsychotic D2 receptor antagonists (never marketed) are also included (Wood & McQuade, 1984). The chemical structures of some aforementioned carbazole-based drugs are presented in Figure 2.

The incorporation of computational methods into *de novo* fragment- or structure-based drug designs enhances faster, economical and environmentally friendly identification of potential top-notch ligands from large databases. In modern drug discovery, the approach includes bio- and cheminformatics, molecular docking analysis, Monte Carlo and molecular dynamics (MD) simulations with biological targets and quantum modelling, widely applied for screening optimized potentials for further phases of drug development such as preclinical and clinical experimental validations. Again, the technique significantly aids extensive and rapid studies of molecular targets and drug interactions, mechanisms of biological events and structure-activity relationships inclusively with representative accuracy and reproducibility to real-life (Prieto-Martínez et al., 2019; Ragno et al., 2020; Schaduangrat et al., 2020; Sliwoski et al., 2014; Tomar et al., 2018). The techniques have been applied to characterize and identify bioactive ligands acting through network pharmacology (Obaidullah et al., 2022; J. Peng et al., 2022; Que et al., 2021) with results validated as good representatives through experimental models (Song et al., 2022). The Ambinter Greenpharma (https://www.ambinter.com/) and IBScreen (https://www.ibscreen.com/) databases are among renowned open-access chemical libraries enriched with freely downloadable natural lead-like small molecules for high throughput screening (Sorokina & Steinbeck, 2020). The libraries have been extensively explored in some recently reported studies for identifying promising candidates, exhibiting network interactive mechanisms amenable to inhibiting some relevant targets for clinical conditions including blood circulation, depression and

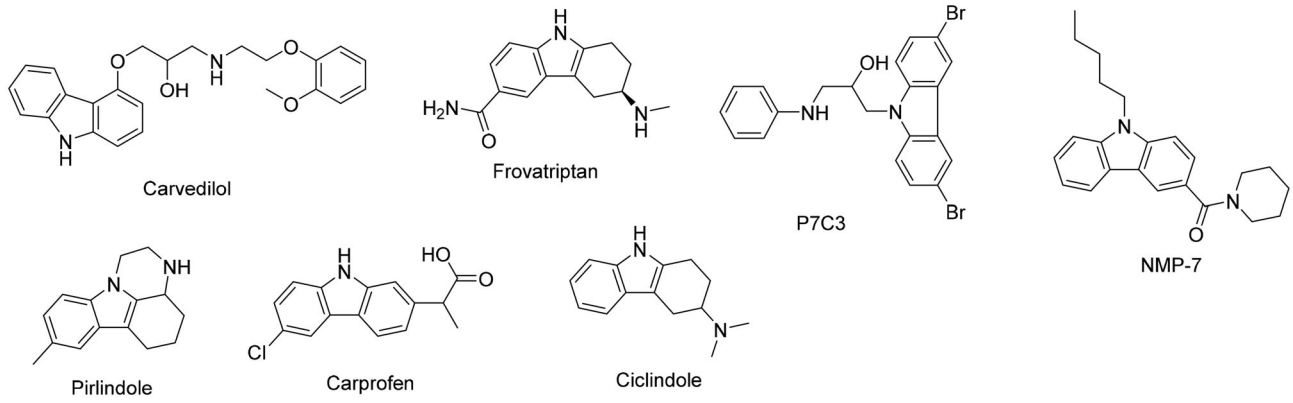


Figure 2. Chemical structure of some carbazole-based drugs.

COVID-19 (Ayipo et al., 2022; Potamitis et al., 2019; Samdani et al., 2022; Shahwar et al., 2022).

Thus, in this study, the potentials of carbazole derivatives (CDs) were investigated for network pharmacology on hSERTs to identify potent antidepressants with improved safety and therapeutic effects. The multi-dimensional inhibitory mechanisms of the database CDs were evaluated for allosteric, competitive and non-competitive interactions with hSERTs (PDB 7LWD; PDB 5I73 and PDB 3GWV) using ligand-protein standard precision (SP) docking analysis. The ligands with consistently higher affinities and better pharmacologically important interactions with the hSERTs than the reference antidepressant drugs were selected for thermodynamic stability and compactness studies through MD simulation while their pharmacokinetics, pharmacodynamics and toxicological profiles were predicted using the Swiss-ADME server (http://www.swissadme.ch/).

Materials and method

Ligand selection and preparation

The Ambinter Greenpharma (https://www.ambinter.com/) and IBScreen (https://www.ibscreen.com/) chemical libraries with over 150,00 and 555,000 screening compounds respectively were searched for carbazole substructures by the input of backbone chemical structure of carbazole alkaloid. The reference hSERT antidepressant medications, (S)-citalopram, fluoxetine and vilazodone were downloaded in SDF files from the PubChem database (https://pubchem.ncbi.nlm.nih.gov/). All the ligand SDF files were imported into Maestro 12.2 workspace for preparation using the LigPrep module of the software (LigPrep, Schrodinger, LCC, New York, NY, 2019). The preparation protocols involve energy minimization, assignment of protonation state by Epik, pH of 7.0 +/- 2.0, geometry and partial atomic charges estimation using optimized potentials for liquid simulations 3e (OPLS-3e) force field, generation of maximum 32 conformers per ligand and other parameters which were set at default, adopting reported procedures (Ayipo et al., 2021; Ayipo et al., 2022; Ayipo et al., 2022; Harder et al., 2016). The minimized ligands in their ready-to-dock protonated states were saved in a LigPrep output folder.

Protein selection and preparation

The protein receptors used for the polypharmacological studies of the carbazole derivatives through molecular interactions were selected from the Research Collaboratory for Structural Bioinformatics Protein Data Bank (RCSB PDB, https://www.rcsb.org/). The Cryo-EM structure of the wild-type hSERT complexed with vilazodone (PDB 7LWD) was selected for the evaluation of mixed competitive and allosteric inhibitory interactions of the ligands (Plenge et al., 2021). Similarly, a crystal structure of the hSERT with *(S)*-citalopram co-crystallized at both central and allosteric pockets (PDB 5I73) (Coleman et al., 2016) was also explored. The third structure additionally considered in this study is the leucine transporter (LeuT), a homolog of hSERT, (PDB 3GWV) in which fluoxetine, the most commonly prescribed SSRI is co-crystallized with a resolution of 2.36 Ð. Several studies have employed the crystal structure to characterize serotonergic antidepressant ligands (Fronza et al., 2017; Immadisetty, 2015; Sundaram et al., 2018). The receptors were prepared separately by importing their retrieved PDB files into the workspace of Maestro 12.2 and following the protocols of the protein preparation wizard (Madhavi Sastry et al., 2013). The correct bond orders were assigned, missing loops filled and protonation states were assigned during the preprocessing stage. These were followed by the optimization, refining, energy minimization and conversion of heavy atoms to relative mean square deviation (RMSD) 0.3Ð using the OPLS-3e force field (Ayipo et al., 2021; Harder et al., 2016). The grid boxes within which the active ligands are expected to be docked were generated for each minimized receptor by selecting the centroid of the workspace ligands, vilazodone, *(S)*-citalopram and fluoxetine for PDBs 7LWD, 5I73 and 3GWV respectively. The x, y and z coordinates of the binding pockets were assigned by default as well as the active site amino acid residues. The prepared grid boxes were saved in zipped files for docking protocols.

Molecular docking analysis

The potentials of the CDs for multi-dimensional network pharmacology against the selected serotonin receptors were studied using the SP module of Maestro 12.2 for ligand-protein molecular docking (Ligand docking, Schrodinger, LCC, New

York, NY, 2019). The prepared CD ligands were evaluated for mixed competitive and allosteric inhibition against hSERTs (PDB 7LWD and PDB 5I73) using the co-crystallized vilazodone and *(S)*-citalopram as templates for active site configuration and docking references. The ligands were also docked against the prepared crystal structure of LeuT, a homolog of SERT (PDB 3GWV) using the co-crystallized SSRI, fluoxetine as a template for active site configuration and docking analysis to evaluate their potency for competitively binding as SSRIs. The inhibitory potentials of the CDs in terms of binding affinity were compared with those of the reference drugs using the docking Gscores in kcal/mol. Similarly, their interactions with essential amino acid residues for the targeted inhibitory expressions were comparatively analyzed together with the references using the 2D and 3D interactive binding poses. In addition to the co-crystallized inhibitors of the selected transporter proteins, escitalopram, fluoxetine and vilazodone which were adopted as positive controls, two carbazole-based FDA drugs, carprofen, a nonsteroidal anti-inflammatory drug and NMP-7, a non-selective cannabinoid receptor agonist/antagonist (anticonvulsant) were included as negative inhibitors for a fair comparison. The docking protocols were validated by redocking the co-crystallized ligands unto the prepared grid box of each receptor and superimposing both poses of the co-crystallized and redocked ligand for the calculation of the RMSD using Maestro 12.2 (Structure alignment/-superimposition, Schrodinger, LCC, New York, NY, 2019). The docking protocol is validated as accurate and reliable if the RMSD values are <2.00 Å (Castro-Alvarez et al., 2017; Ramírez & Caballero, 2018).

Molecular dynamics

To further study the structural alterations in the physiological environment and thermodynamic stability influenced on the receptors by the selected ligands in the absence of experimental validation, the docking complexes were subjected to MD simulations. The Desmond programme from the Schrödinger LLC package dynamics software package was used to run the simulations with the OPLS-3e force field (Chaudhari et al., 2022; D. E. Shaw Research & Schrödinger Release, 2021). A box for an orthorhombic periodic simulation was created, and ligand-protein complexes were configured inside the box. The simulation cell was extended by 10 Å to permit free movement (Hart et al., 2022). The Single-point charge (SPC) water solvation model was applied, and the steepest descent algorithm was used to perform the energy minimization step to accomplish the threshold of 1 kcal/mol/Å. The reversible reference system propagator algorithms (RESPA) integrator was applied in the numerical integration, with a short-range/bonded interaction updated every 2 picoseconds (ps) and a long-range/-non-bonded interaction updated every 6 ps (Ivanova et al., 2018). For long-range electrostatic interactions, the Smooth Particle Mesh Ewald approach with a tolerance of 1e-09 was utilized, whereas a cut-off radius of 9 was used for short-range electrostatic interactions. Each simulation was run for 100 ns, and each trajectory was saved after 100 ps. Subsequently, the output of MD generated by Desmond, which included the RMSD, root mean square fluctuations (RMSF), hydrogen bond analysis, principal component analysis (PCA), secondary structure analysis and radius of gyration (RGyr) were inferred to deduce stability (Ivanova et al., 2018).

Estimation of molecular mechanics-generalized Born surface area

The post-dynamic molecular mechanics-generalized Born surface area (MMGB/SA) was used as a hybrid energy calculation method to estimate the changes in molecular mechanics, electrostatic, entropic, nonpolar and van der Waals energy contributions. Both ligand-bound and unbound states are considered for the approximations (Immadisetty, 2015). The MM/GBSA binding free energy computation for the calculation of ligand-binding affinity was executed by the thermal_mmgbsa.py script using MD trajectories (Hart et al., 2022).

Physicochemical, pharmacokinetics, pharmacodynamics and toxicity predictions

The physicochemical, pharmacodynamics, pharmacokinetic and toxicological properties of the selected ligands were predicted *in silico* using the pkCSM ADMET descriptors algorithm, with the input of the ligands' SMILE files (Pires et al., 2015). The predictions were benchmarked with the BDDC and Lipinski's rule of five (RO5). Additionally, this program theoretically predicts how well drugs are absorbed, soluble (log S), bioavailable (Caco-2 cell monolayer permeability), gastrointestinal (GI) absorption in humans, skin permeability level, and the substrate or inhibitor of permeability glycoprotein (P-gp) efflux pump. The topological polar surface area (TPSA) as a critical determinant of fractional absorption was estimated by pkCSM (Pires et al., 2015). The penetrability across the blood-brain barrier (BBB) and the central nervous system (CNS), as well as volume of distribution and fraction unbound, were also among the distribution descriptors. The metabolic factor was predicted based on the potential for inhibitory action against essential cytochrome P450 (CYP) isoforms. The excretion potential of the ligands was predicted using parameters such as total clearance and renal OCT2 substrate, whereas their toxicity was assessed through mutagenicity potential (AMES toxicity), hERG toxicity, skin toxicity, and liver toxicity. Promising candidates with ideal potentials for druggability and pharmacokinetic properties were identified as hits for future studies.

Results and discussion

Molecular docking analysis

A total number of 1100 carbazole derivatives were retrieved from the search of the databases and 4801 minimized conformers were generated upon ligand preparation. Out of these, only 2098 minimized conformers with appropriate size and structure for binding to the active pockets of the prepared receptors were successfully docked. The docking procedure validated through the superimposition of both co-crystallized and redocked ligands of the selected crystal structures produced

good alignments. These are indicated by low RMSD values of 0.6952, 0.8630 and 1.4353 Ð for the lowest energy poses of vilazodone, ritanserin and fluoxetine when redocked onto the active pockets of their respective crystal structures (Figure 3). The values are well below 2 Ð, thereby validating the docking protocols as accurate, precise and reliable (Ayipo et al., 2022; Castro-Alvarez et al., 2017; Ramírez & Caballero, 2018).

From the molecular docking analysis of the ligands with the selected serotonergic targets, the selected CDs and reference ligands were arranged in ascending order of binding affinities represented by the docking Gscore (kcal/mol). The results show that not less than 90 CDs display higher docking scores for affinity than the reference co-crystallized drugs against each receptor (Table 1 and Supplementary Table S1). Four database CDs annotated as **STOCK3S-30866**, **STOCK1N-37454**, **STOCK1N-40491** and **STOCK2S-81285** with consistently higher docking scores than the reference clinical inhibitors, **vilazodone, *(S)*-citalopram** and **fluoxetine** across all the probed receptors were selected for further analysis. The ligands demonstrated potential for stronger competitive and allosteric binding to the serotonergic targets than some currently prescribed clinical inhibitors. These further support the chance for optimized bioactive hits for hit-to-leads development, typical of high throughput virtual screening (Gangadharan et al., 2017). Similar results have also been reported for some database ligands against some serotonergic targets for depression (Ayipo et al., 2022; Ayipo et al., 2022; Y. Peng, Zhao, et al., 2018). The two carbazole-based drugs adopted as negative inhibitors in the docking analyses, **NMP-7** and **carprofen** (CB receptor agonist/antagonist and NSAID respectively) consistently scored the lowest as expected, further supporting the validity of the docking analysis. The latter did not even dock onto the active pockets of all the selected receptors possibly due to its large structural size and rigidity (Guedes et al., 2014). Again, these support the selectivity of the receptors towards the highlighted top-ranked database CDs and pose them as putative serotonergic inhibitors for further analyses. In addition to the binding affinities, the mechanisms of inhibition of the selected CDs against the targets in mimicry to the renowned inhibitors were importantly analyzed through the interactive binding poses with amino acid residues at the active pockets of the targets.

Competitive and allosteric inhibitory interactions of carbazole derivatives with hSERT in comparison with vilazodone

The characterization of vilazodone by molecular pharmacology and structural elucidation indicated its versatile therapeutic features as an allosteric inhibitor of the hSERT additionally to the competitive inhibition commonly demonstrated by all SSRIs. The crystal structure (PDB 7LWD) from the RCSB PDB displays the drug within a unique binding

Table 1. Docking scores of selected carbazole derivatives and reference drugs with hSERTs.

	SP Gscore (kcal/mol)			
Title	PDB 7LWD	PDB 5I73 (Central)	PDB 5I73 (Allosteric)	PDB 3GWV
STOCK3S-30866	−9.523	−9.282	−8.153	−8.569
STOCK1N-37454	−9.587	−9.103	−8.397	−7.715
STOCK1N-40491	−9.466	−9.315	−7.897	−7.625
STOCK2S-81285	−8.938	−8.379	−8.153	−7.401
Fluoxetine	−7.965	−9.660	−7.462	−6.446
Escitalopram	−8.019	−9.890	−6.896	−5.008
Vilazodone	−7.828	−8.966	−8.875	−5.389
NMP-7	−6.314	−8.378	−5.936	−5.292
Carprofen	ND	ND	ND	ND

ND: Not docked.

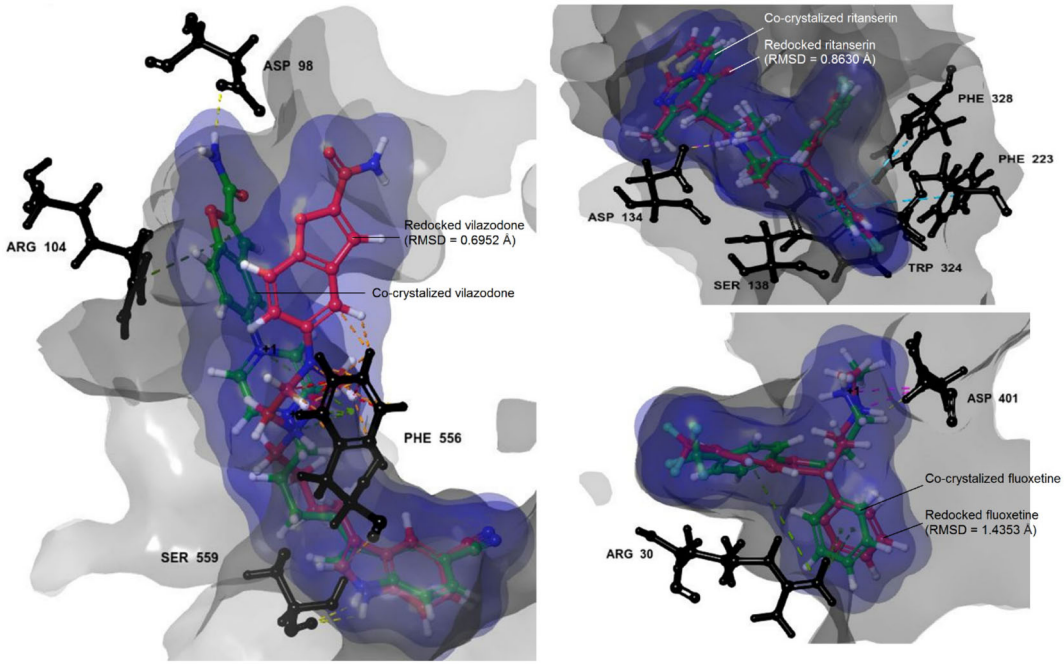


Figure 3. Superimposition of co-crystallized and redocked ligands at the active pockets of selected receptor crystal structures. All produced good alignment with RMSD values < 2 Ð, validating the protocols as being precise and reliable.

pocket with expanded boundaries of the extracellular vestibule (Plenge et al., 2021). According to the depositor of the crystal file and relevant studies, the active site S1 of the protein is inclusively constituted by Tyr 95, Asp 98, Ile 172, Tyr 175, Tyr 176, Phe 341 and Thr 497. while the allosteric site S2 is occupied by Arg 104, Phe 335, Glu 493, Glu 494, Tyr 495 and Pro 499 among the essential amino acid residues for antidepressant effects of ligands (Immadisetty, 2015; Plenge et al., 2021). The binding poses generated from the docking protocols (Figure 2) indicate that vilazodone formed a hydrophilic π-cation interaction with Phe 341 through its protonated NH group and hydrophobic π-π interaction with Tyr 176 through its aromatic moiety, indicating its potential for competitive inhibition as an SSRI (Plenge et al., 2021). Additionally, it formed hydrophobic interactions with Arg 104, Phe 335, Glu 493 and Glu 494 among critical residues for allosteric binding (Plenge et al., 2021). The IBScreen ligand, **STOCK3S-30866** consistently displayed such relevant interactions including H-bonding to Asp 98 through the NH, π-cation to Phe 335 through its protonated NH, π-π interactions to Tyr 176 and Phe 335 within the active site S1 for competitive mechanism, then hydrophobic interactions with the characteristic site S2 residues for allosteric binding including Glu 493 and Glu 494. Other selected ligands, **STOCK1N-37454, STOCK1N-40491** and **STOCK2S-81285** also consistently displayed similar interactions (Figure 4; Supplementary Figure S1). Such important binding interactions for characterizing a drug as both a competitive and allosteric inhibitor have been verified through experimental studies. For instance, Lu AF60067, a SERT inhibitor displayed high affinity to the site S2 allosterically coupled with strong binding to the central active site S1 pocket, and reportedly potentiated by imipramine to boost the hippocampal 5-HT level in rat model experiment (Plenge et al., 2020). Similarly, a crystal structure of SERT complexed with an SSRI, S-citalopram (PDB 5I73) contains two inhibitors that bound to the respective S1 and S2 sites of the SERT, supporting the plausibility of a second molecule binding to both primary and allosteric pockets (Coleman et al., 2016; Jean, 2017). These demonstrations conform with the possibility of polypharmacology (one-drug-dual-target) through competitive and allosteric binding to SERT, an effective treatment for MDD (Plenge et al., 2020, 2021). Thus, the compounds are worthy of further assessment as potential candidates for mixed competitive and allosteric inhibition of hSERT for enhanced therapeutic effects and safety.

Competitive and allosteric inhibitory interactions of carbazole derivatives with hSERT in comparison with (S)-citalopram

Mechanistically, *(S)*-citalopram is a renowned SSRI that is characterized by binding competitively to the central active pocket of the hSERTs. Recently, studies have shown that the antidepressant additionally binds strongly to the extracellular vestibule (allosteric pocket) of the hSERTs and other serotonergic receptors in a non-competitive pattern, thereby exhibiting synergistic inhibitory effects on the transporter (Coleman et al., 2016; Park & Sung, 2019). Supportively, an X-ray structure of the hSERT containing the drug co-crystallized at both central and allosteric pockets of the receptor has been released to the RCSB PDB (PDB 5I73), demonstrating an enhanced antidepressant performance through monoligand-based polypharmacology (Coleman et al., 2016; Plenge et al., 2020). The CDs were therefore investigated for the potential to mimic *(S)*-citalopram or perform better through molecular interactions with the hSERT co-crystallized with the drug (PDB 5I73). The docking scores have supported the selected CDs as stronger allosteric binders and comparative interactors of the hSERT relative to the renowned antidepressants. The 2D and 3D interaction diagrams of the selected CDs at the central pocket of the hSERT in comparison with a known inhibitor, *(S)*-citalopram, are presented in Figure 5. It could be observed that the tertiary amine group of the co-crystallized drug, *(S)*-citalopram occupied the site S1 engaging in hydrophilic interactions with the conserved amino acid residues, Asp 98 and Tyr 95 through H-bonding, π-cation and salt bridge formations. These are crucial for antidepressant potency (Coleman et al., 2016). The selected CDs also exhibited similar bonding interactions. For instance, **STOCK3S-30866** formed a salt bridge interaction with Asp 98 through its protonated amine group. It also displayed hydrophobic π-π and non-bonding van der Waals interactions with Tyr 176 and Tyr 95 respectively, supporting its competitive binding typical of SSRI. Similarly, **STOCK1N-37454** engaged the same crucial Asp 98 *via* H-bonding and salt bridge formation through its NH group, representing hydrophilic interactions consistently with *(S)*-citalopram. The ligand additionally bonded to Arg 104, a residue at the extracellular vestibule for conformational stabilization of the protein (Plenge et al., 2021) through a π-cation interaction. The central active pocket occupied by the selected ligands and reference drug contains other antidepressant-inclined pharmacologically essential amino acid residues such as Ser 336 which coordinates the ligand interaction network with Na^+ and Cl^- ions, essentially for substrate binding and transport (Coleman et al., 2016). Other relevant amino acid residues to competitive binding such as Ile 172, Tyr 175, Phe 341 and Thr 497 (Immadisetty, 2015; Plenge et al., 2021) are equally available at the central active binding pocket exhibiting van der Waals interactions with the ligands. These support the ligands as promising competitive inhibitors of the active site of hSERT, consistently with *(S)*-citalopram.

The interactions of the CDs and the co-crystallized reference drug, *(S)*-citalopram at the allosteric pocket of hSERT (PDB 5I73) are displayed in Figure 6. Accordingly, the residues Gln 332 and Phe 335 occupying the transmembrane 6 (TM6) Glu 493, Glu 494 and Tyr 495 localised on TM10, Phe 556 and Tyr 579 on the TM11 and TM12 respectively constitute the allosteric binding site. Whereas, Gln 332 and Tyr 495 essentially form the 5-HT transport cavity (Immadisetty, 2015; Plenge et al., 2021). In the diagrams (Figure 6), *(S)*-citalopram bonded to Phe 335 through a hydrophobic π-π stacking utilizing its cyano-bearing benzene group. **STOCK1N-37454** also exhibited similar hydrophobic interaction through its fused aromatic rings and hydrophilic π-cation to Arg 104, essentially for the protein conformational stability (Plenge et al., 2021),

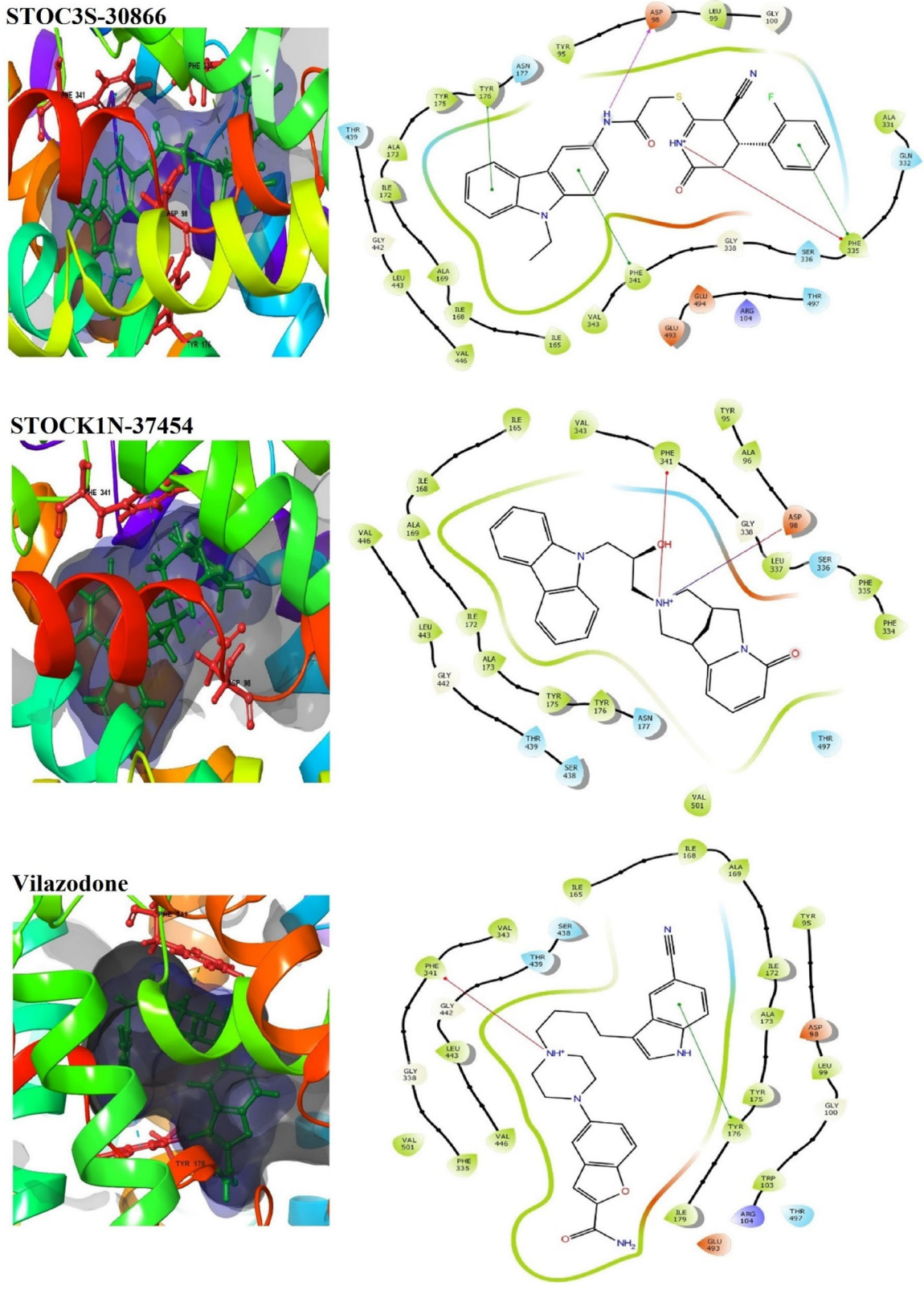


Figure 4. Competitive binding interactions of STOCK3S-30866 and STOCK1N-37454 with central active and allosteric sites of hSERT (PDB 7LWD) in comparison with vilazodone. Bonding interactions: H-bonding (magenta arrow), π-cation (blue line), salt bridge (red-blue line) and π-π stacking (green line).

while **STOCK3S-30866** displayed electrostatic H-bonding and salt bridge formation with Glu 493 on TM10. The potential of the ligands to bind to both allosteric and central active sites hypothetically supports a potent inhibition through synergistic effects. In addition to the putative antidepressant pharmacology, such interactions are amenable to overcoming treatment resistance, loss of efficacy and minimal undesired side effects (S. I. Berger & Iyengar, 2009; Plenge et al., 2021).

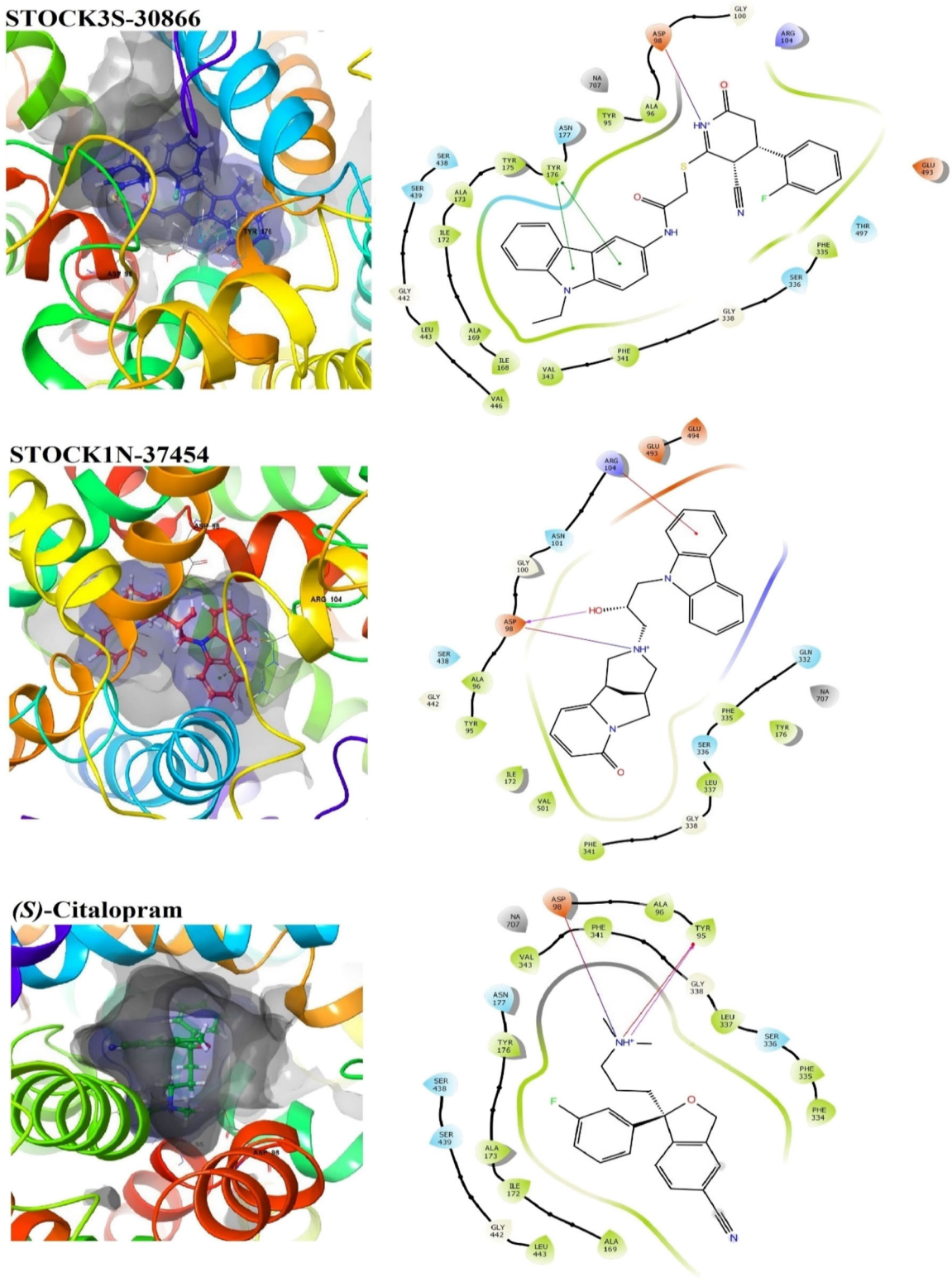


Figure 5. Interaction poses of STOCK3S-30866 and STOCK1N-37454 as competitive binders of the central pocket hSERT (PDB 5I73) in comparison with *(S)*-citalopram. Bonding interactions: H-bonding (magenta arrow), π-cation (blue line), salt bridge (red-blue line) and π-π stacking (green line).

Competitive inhibitory interactions of carbazole derivatives with a homolog of SERT in comparison with fluoxetine

Accordingly, all SSRIs are competitive inhibitors of the SERT (Plenge et al., 2021). The potentials of the selected CDs for competitive inhibition against the LeuT, a bacterial homolog of hSERT (PDB 3GWV) were illustrated by bonding and non-bonding 2D and 3D binding interaction poses (Figure 7; Supplementary Figure S2) to support the docking results. As reported by the author of the crystal structure, the active binding pocket of the receptor is constituted by key amino acid residues for SSRI pharmacology including Leu 25, Gly 26, Leu 29, Arg 30, Gln 34, Tyr 108, Ile 111, Phe 253, Ala 319, Phe 320, Asp 401 and Asp 404 (Zhou et al., 2009). The selected binding pocket for docking analysis correctly conforms to the

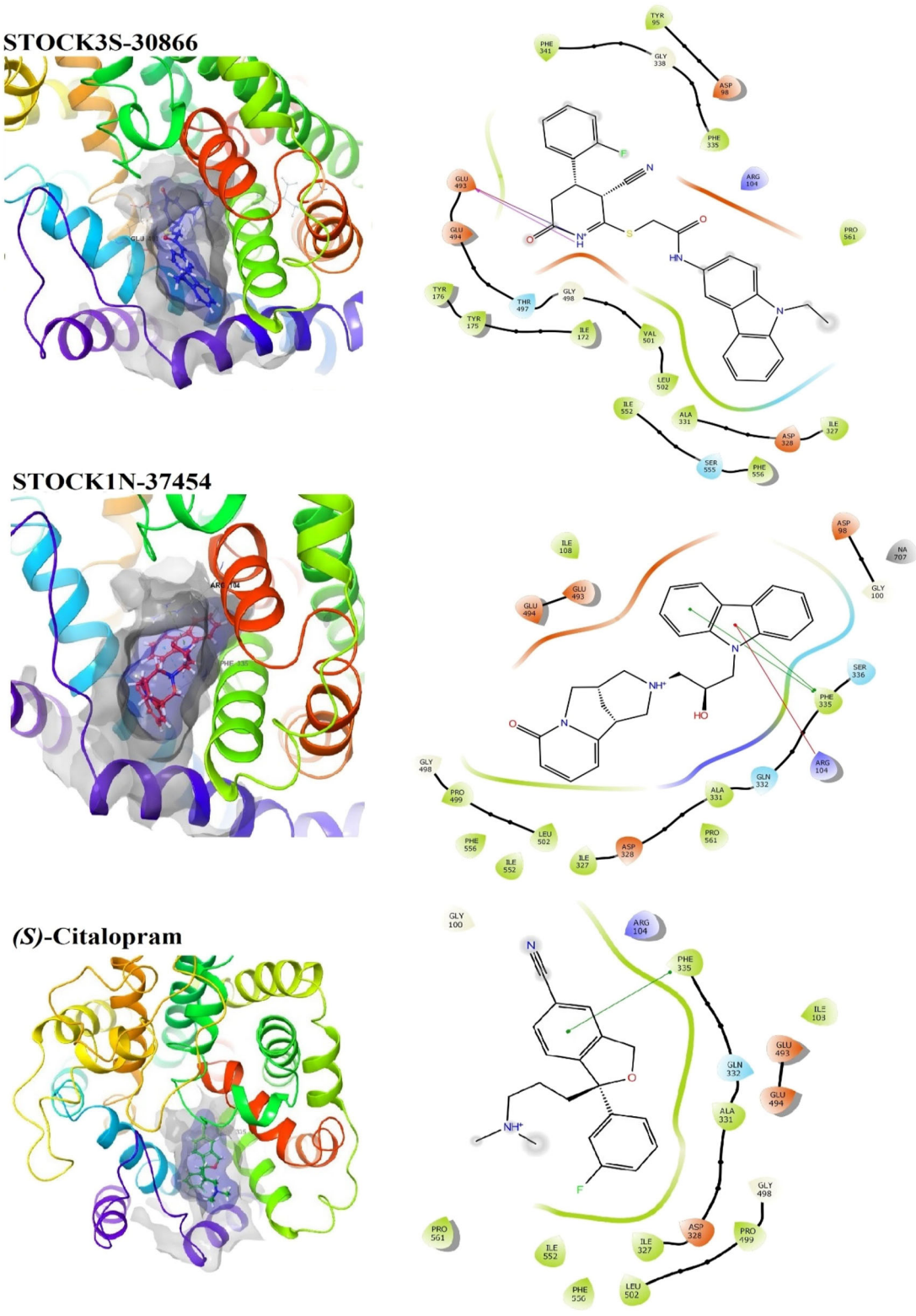


Figure 6. Interaction poses of STOCK3S-30866 and STOCK1N-37454 as non-competitive binders of the allosteric pocket of hSERT (PDB 5I73) in comparison with *(S)*-citalopram. Bonding interactions: H-bonding (magenta arrow), π-cation (blue line), salt bridge (red-blue line) and π-π stacking (green line).

same sets of amino acid residues in similar arrangements. For instance, in the adopted reference SSRI, **fluoxetine** bound to the extracellular vestibule in the receptor with its F atom enclosed within the halogen-binding pocket (HBP) and in bonding contacts with Leu 25, Gly 26, Leu 29, Arg 30 and Tyr 108. Its phenyl moiety was surrounded by Ala 319 and Phe 320 along the tip of the extracellular loop 4 (EL4) hairpin, and Leu 400 and Asp 401 from the transmembrane α-helix 10 (TM10) on the extracellular side. The drug engaged Asp 401 for H-bonding through its NH and formed a salt bridge with the protonated NH along the cytoplasm, and then a π-cation interaction with Arg 30 through its second phenyl moiety

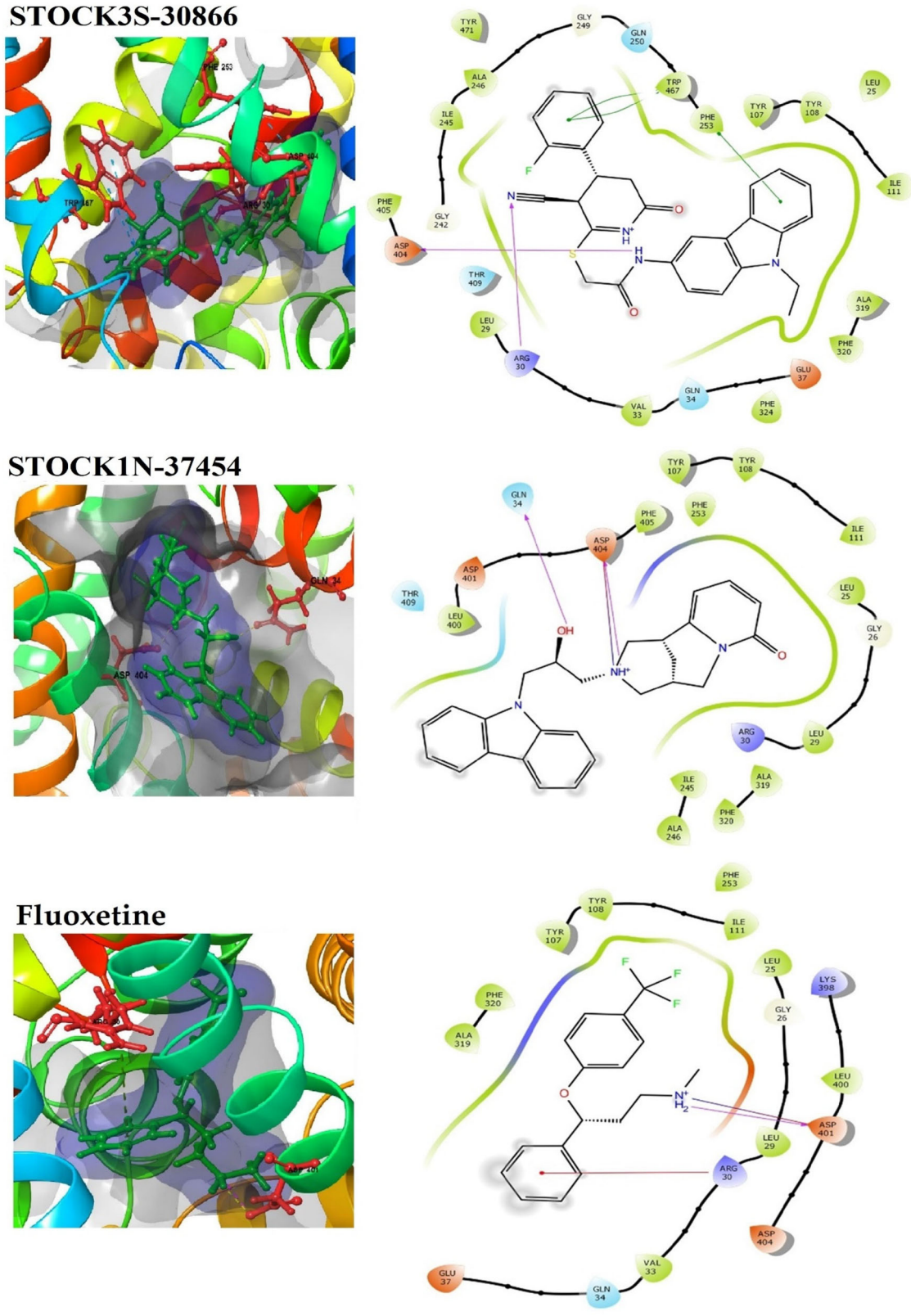


Figure 7. Interaction poses of STOCK3S-30866 and STOCK1N-37454 at the active site of hSERT (PDB 3GWV) as putative SSRIs in comparison with fluoxetine. Bonding interactions: H-bonding (magenta arrow), π-cation (blue line), salt bridge (red-blue line) and π-π stacking (green line).

consistently as reported (Zhou et al., 2009). The selected ligands under probe, **STOCK3S-30866, STOCK1N-37454, STOCK1N-40491** and **STOCK2S-81285** also demonstrated many similar interactions with some additions such as H-bond to Gln 34 by **STOCK1N-40491**, salt bridges to Gln 34 and Asp 404 by **STOCK1N-37454** and **STOCK2S-81285** respectively, supporting their higher affinities. These are consistent with a template study by Zhou et al., 2009, where three SSRIs, R-fluoxetine, S-fluoxetine and sertraline were probed for selective inhibitory interactions on the SERT. The three SSRIs reportedly bound to the

receptor at the same position and in a similar manner to exert SSR inhibitory effects as confirmed experimentally (Zhou et al., 2009), in much the same patterns as shown by the selected ligands herein studied. This further support the inhibitory interactions of the selected ligands as promising SSRIs amenable for experimental validation.

Molecular dynamics

To establish the structural deviation of the docked protein and inhibitor complex, the molecular dynamics trajectories were examined and the RMSD of the docked complex molecules was evaluated to figure out the deviations. The determination of protein RMSD offers accurate predictions of the system's conformational stability (Ahmad et al., 2022). The variations of protein atoms from their initial locations are predicted as part of the RMSD calculation. The protein Cα RMSD was computed for the 100 nanoseconds (ns) simulation run that generated 1000 frames of the Apo protein and the protein-ligand complex structures as shown in Figure 8. The average, maximum, and minimum RMSD values along with other assessments are given in Table 2.

Root mean-squares deviation (RMSD)

The RMSD of the folded protein Cα atoms derived from the simulated trajectory of the protein-ligand complex reveals their deviation from initial conformations in a dynamic environment upon binding. A larger RMSD value for protein Cα atoms implies unfolding, whereas a lower value favours compactness. The modest variation of the backbone RMSD further supports the protein-ligand complex's equilibration. The difference between the greatest and least RMSD indicates backbone deviation. The overall RMSD of the 7LWD-STOCK1N-37454 and 7LWD-STOCK3S-30866 complexes revealed that fluctuations in the range of 1.368 to 3.439 Å, governed the complex's stability and consistency in a dynamic environment. In the case of the standard drug 7LWD-Vilazodone complex, the minimum, maximum, and average were found to be 1.317 Å, 2.850 Å, and 2.410 Å, respectively, which are comparable to the Apo protein. Both of the docked complexes with 7LWD protein showed straight lines and had decreased degrees of deviation after the initial variation driven by equilibration. Although some oscillations were seen, the RMSD analysis did not find them to be noteworthy (Figure 8(a)). The results of the RMSD analysis for the 5I73 protein (central) revealed that the Apo protein initially elevated its RMSD profile, possibly owing to the presence of a high level of flexibility. It then stabilizes rapidly after 40 ns MDS until 70 ns, after which it increases slightly until the end of the simulation. The RMSD descriptors of the complexes 5I73-STOCK1N-37454 (mean RMSD = 1.831 Å) and 5I73-Escitalopram (mean RMSD = 1.966 Å) showed a similar RMSD profile and sustained stability with little fluctuation. The STOCK1N-37454 instance showed a few minor deviations.

The adaptation of the binding site may be the cause of these discrepancies. The maximum RSMD (∼2 Å) was observed between 45 and 80 ns, which corresponds to the Apo-protein RMSD. In comparison to the Apo protein, the RMSD deviations in the 5I73-STOCK1N-37454 complex are marginally lower (Figure 8(b)). In 5I73 protein (allosteric) complexes, a parallel RMSD trend was found; both 5I73-STOCK1N-37454 and 5I73-Escitalopram complexes displayed a matching RMSD curve, except for 5I73-STOCK1N-37454 having an RMSD of 2.353-2.673 Å in the range of 21 ns to 54 ns (Figure 8(c)). The complexes' RMSD values show that the protein structure is unchanged by the inhibitor's binding when compared to the 3GWV Apo protein. The conformational stability of 3GWV complexes with STOCK1N-37454 (mean RMSD = 1.750) and STOCK3S-30866 (mean RMSD = 1.658) demonstrates that they have a lower RMSD value than the free protein (mean RMSD = 1.937 Å) and the standard drug 3GWV-Fluoxetine complex (mean RMSD = 2.027 Å). It is conceivable that the complexes attained stability and consistency in a dynamic environment (Figure 8(d)).

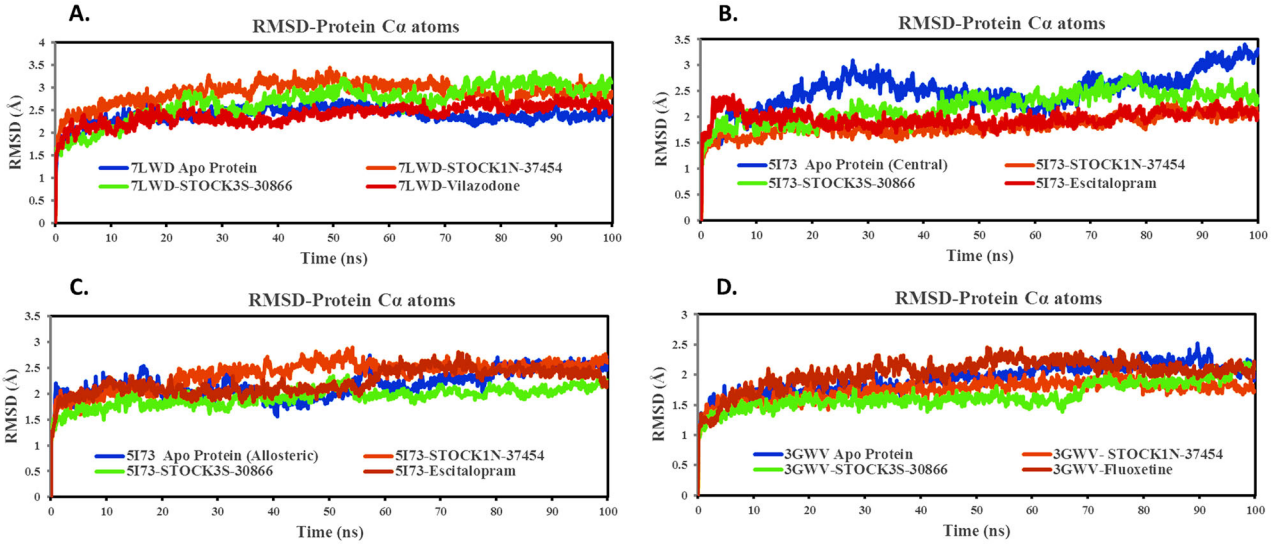


Figure 8. Time-dependant RMSD analysis of Apo protein and in complex with STOCK1N-37454, STOCK3S-30866 and standard drug ((a) 7LWD, (b)5I73 (central), (c) 5I73 (allosteric) and (d) 3GWV) data obtained from MD simulation trajectories.

Table 2. Minimum, maximum and average, RMSD, RMSF, RGyr and MM-GBSA binding free energy values of proposed inhibitors and standard drugs.

	7LWD Apo Protein	7LWD-STOCK1N-37454	7LWD-STOCK3S-30866	7LWD-Vilazodone	5I73 Apo Protein	5I73-STOCK1N-37454	5I73-STOCK3S-30866	5I73-Escitalopram	5I73 Apo Protein	5I73-STOCK1N-37454	5I73-STOCK3S-30866	5I73-Escitalopram	3GWV Apo Protein	3GWV-STOCK1N-37454	3GWV-STOCK3S-30866	3GWV-Fluoxetine
					(Central)				(Allosteric)							
Protein C-α atoms RMSD (Å)																
Min	1.060	1.368	1.505	1.317	1.090	1.054	1.032	1.306	1.186	1.198	1.008	1.088	1.069	0.904	0.885	1.025
Max	2.799	3.439	3.359	2.850	3.401	2.318	2.880	2.431	2.738	2.890	2.360	2.802	2.518	2.127	2.197	2.459
Average	2.392	2.889	2.693	2.410	2.502	1.831	2.201	1.966	2.174	2.378	1.936	2.221	1.937	1.750	1.658	2.027
Protein C-α atoms RMSF(Å)																
Min	0.510	0.442	0.500	0.513	0.465	0.447	0.405	0.449	0.449	0.446	0.425	0.435	0.416	0.411	0.404	0.351
Max	4.255	4.958	5.321	4.932	8.262	5.949	5.321	4.118	5.010	6.579	4.393	6.177	7.647	5.042	4.705	4.179
Average	1.114	1.088	1.190	1.229	1.220	1.021	1.025	0.971	1.066	1.017	0.961	1.009	0.870	0.882	0.884	0.890
Hydrogen bond analysis																
Min	–	1.00	1.00	1.00	–	1.00	1.00	1.00	–	1.00	1.00	1.00	–	1.00	1.00	1.00
Max	–	3.00	5.00	6.00	–	2.00	3.00	2.00	–	2.00	4.00	2.00	–	2.00	4.00	3.00
Average	–	1.72	3.19	3.59	–	1.36	1.48	0.93	–	0.89	1.63	1.31	–	1.03	3.40	1.47
Radius of gyration (Å)																
Min	3.835	3.872	5.419	4.032	3.554	3.75	4.687	3.59	4.628	3.934	4.049	3.662	4.223	3.708	5.189	3.923
Max	4.317	4.351	5.978	4.803	4.365	4.494	5.553	3.793	5.271	4.983	4.829	3.974	4.475	5.207	6.178	4.355
Average	4.07	4.04	5.69	4.40	4.043	4.141	5.157	3.687	4.845	4.655	4.579	3.882	4.367	4.50	5.89	4.195
MM-GBSA binding free energy (kcal/mol)																
Min	–	−59.01	−84.80	−51.42	–	−58.93	−102.14	−38.83	–	−58.09	−84.15	−60.22	–	−60.03	−76.69	−43.78
Max	–	−74.70	−102.52	−69.68	–	−81.34	−114.99	−58.91	–	−82.18	−109.43	−74.70	–	−85.79	−85.75	−55.91
Average	–	−65.66	−92.96	−59.27	–	−71.25	−107.39	−47.46	–	−68.46	−96.14	−69.39	–	−75.32	−81.03	−50.51
Secondary structure analysis																
% Helix	51.67	51.51	51.65	52.14	55.93	55.16	53.90	55.34	54.99	53.38	54.80	54.20	64.16	64.60	62.88	60.08
% Strand	0.56	0.00	0.67	0.70	0.49	0.66	0.68	0.50	0.62	0.68	0.63	0.51	0.06	0.07	0.05	0.31
% Total SSE	52.23	51.51	52.31	52.84	56.43	55.82	54.58	55.84	55.62	54.06	55.43	54.71	64.21	64.66	62.93	60.39

Root mean-squares fluctuations (RMSF)

The stability of the protein-ligand complex and the overall flexibility of the protein amino acids are predicted using root mean square fluctuations (RMSF). The bigger variations generally imply substantial fluctuations in the side chain residues, as well as probable ligand dissociation or unfavourable ligand interactions at the binding site (Hart et al., 2022). The difference between maximum and average, as well as average and minimum, may provide information on the fluctuation of amino acid residues in the MD simulation. The difference between maximum and average, and, average and minimum were found to be 3.87 Å and 0.646 Å; 4.131 Å and 0.69 Å; 3.703 Å and 0.716 Å; 4.928 Å and 0.574 Å; 4.296 Å and 0.62 Å; 3.147 Å and 0.522 Å; 5.562 Å and 0.571 Å; 3.432 Å and 0.536 Å; 5.168 Å and 0.574 Å; 4.16 Å and 0.471 Å; 3.821 Å and 0.48 Å; 3.289 Å and 0.539 Å in case of STOCK1N-37454, STOCK3S-30866 and standard drugs (Vilazodone, Escitalopram and Fluoxetine) with 7LWD, 5I73 (Central), 5I73(Allosteric), and 3GWV proteins respectively (Figure 9(a–d)). In addition, the variation of amino acid residues 131–134 in the 3GWV-STOCK1N-37454 complex and 140–144 in the 7LWD-STOCK1N-37454 complex is more than 3 Å. While major fluctuation is detected in STOCK3S-30866, residual index 141–143 and 156–159, 474–576 in complex with 7LWD, and 3GWV proteins, respectively, which is away from the binding site. In both the central and allosteric 5I73 protein complex, a higher RMSF peak is observed in the range of 134–147, C and N terminals. The low values observed at the binding site probably explain the evaluated complex's stability over simulation time.

Hydrogen bond analysis

Intermolecular hydrogen bonding between proteins and ligands is essential for the stability of protein-ligand complexes. Throughout the 100 ns simulation period, the stability of the hydrogen bond network formed between STOCK1N-37454 and STOCK3S-30866 with 7LWD, 5I73, and 3GWV proteins is calculated and shown in Figure 10(a–d). STOCK3S-30866 in complex with 7LWD and 3GWV proteins exhibited 3.19 and 3.40 mean hydrogen bonds, respectively, indicating the strength and binding affinity, whereas the standard drugs 7LWD-Vilazodone and Fluoxetine in 3GWV-Fluoxetine complexes exhibited 3.59 and 1.47 mean hydrogen bonds, respectively, throughout the 1000 MD trajectories. STOCK3S-30866 had the highest hydrogen bonding in both central and allosteric 5I73 proteins when compared to the standard drug Escitalopram, implying a higher binding affinity. The residues Tyr175, Tyr176, Phe335, and Thr497 form the most STOCK3S-30866 hydrogen bonds in the 7LWD protein, while the 3GWV protein forms strong hydrogen bonds with the amino acids Arg30, Gln34, Glu37, and Asp404. According to hydrogen bond analysis, STOCK1N-37454 has less hydrogen bonding than STOCK3S-30866 because it forms the most hydrophobic (π-π interactions) with 7LWD and 3GWV proteins, as shown in Figure S3 (Supplementary information). These findings imply that STOCK3S-30866 forms more hydrogen bonds with several critical residues at the binding site, whereas another complex has one to two residues engaged in direct hydrogen bonding. In STOCK3S-30866, direct hydrogen bonding involves Tyr95, Asp98 and Tyr176, and Glu493 and Thr497 *via* central 5I73 proteins and allosteric 5I73 proteins, respectively. In the case of STOCK1N-37454, the maximum of 2 hydrogen bonds was formed with 5I73 and 3GWV, while 7LWD formed 3 hydrogen bonds each. However, the average number of hydrogen bonds formed with 7LWD, central 5I73, allosteric 5I73, and 3GWV was 1.72, 1.36, 0.89, and 1.03, respectively, suggesting that hydrogen bond formation events occurred moderately with STOCK1N-37454 and it could potentially be stabilized by hydrophobic as well as ionic interactions (Supplementary information, Figure S4).

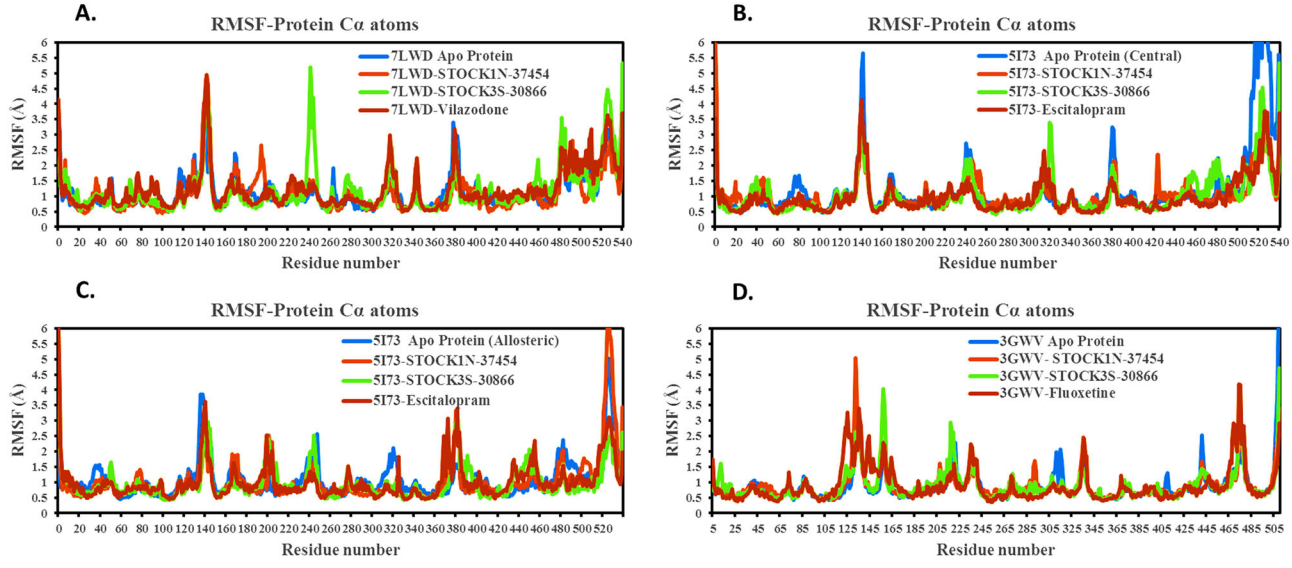


Figure 9. Individual amino acids RMSF of Cα atom OF Apo protein and in complex with STOCK1N-37454, STOCK3S-30866 and standard drug ((a) 7LWD, (b) 5I73 (central), (c) 5I73 (Allosteric) and (d) 3GWV) data from obtained MD simulation trajectories.

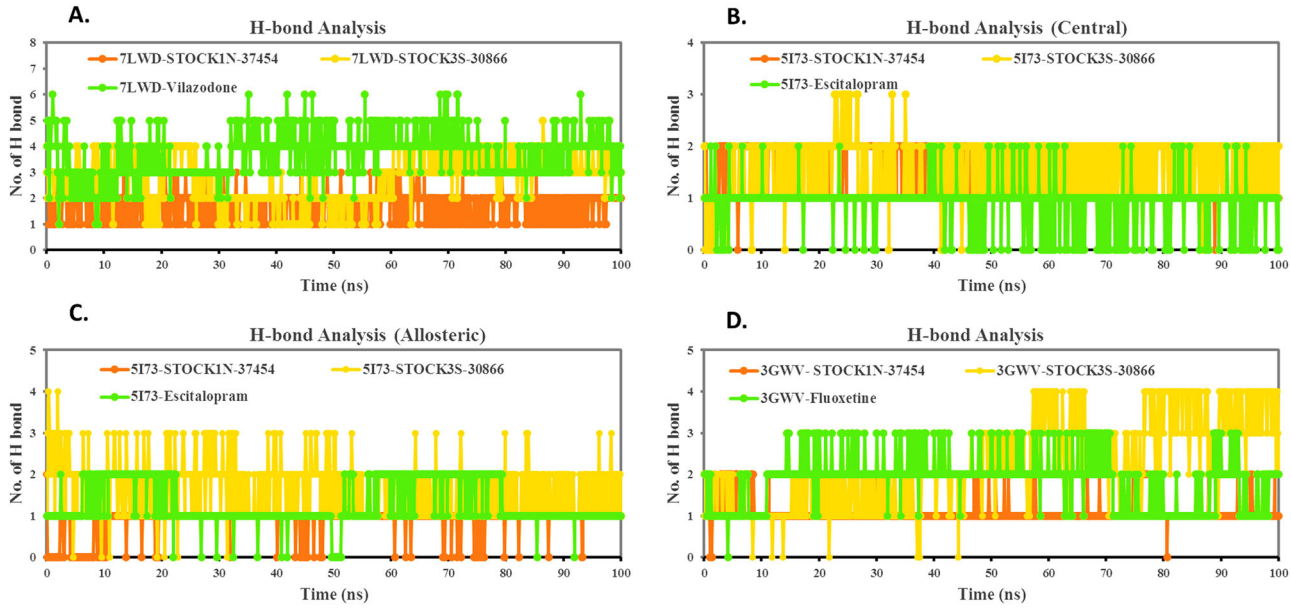


Figure 10. Time-dependent Hydrogen bond analysis of different proteins in complex with STOCK1N-37454, STOCK3S-30866 and standard drug ((a) 7LWD, (b) 5I73 (central), (c) 5I73 (allosteric) and (d) 3GWV) data obtained from MD simulation trajectories.

Radius of gyration (RGyr)

Another criterion for judging the root mean square distance of a group of atoms from their common centre of mass is the examination of the RGyr, which provides insight into the overall tightness of the system (Ahmad et al., 2022). On analyzing the RGyr plot, we have interpreted that the RGyr of the Apo 7LWD, 5I73, and 3GWV proteins was in the range of 3.59 Å to 6.178 Å (Figure 11). STOCK3S-30866 bound with all three proteins has a higher RGyr than STOCK1N-37454, except for the 5I73 allosteric protein, where the initial 20 ns RGyr is higher in STOCK1N-37454. After that, a parallel RGyr was observed. The uniform pattern of RGyr is observed in STOCK3S-30866 in a complex with 7LWD and 5I73 proteins, whereas slight variation is shown in the 3GWV protein around 0–20 ns. The RGyr of the STOCK1N-37454-3GWV complex system was initially down for 3 ns, and the RGyr remained around 4.18 Å until 69 ns, after which a minor fluctuation was observed, followed by a stable RGyr after 86 ns. Therefore, the RGyr plot's pattern against time simulation and minimal fluctuation explained that the residual backbone and folding of all proteins, 7LWD, 5I73, and 3GWV remained constant upon binding with STOCK1N-37454 and STOCK3S-30866, respectively (Figure 11).

Molecular mechanics-generalized Born surface area binding free energy analysis

The binding energy of any small molecule may indicate its affinity for a protein. MMGB-SA is a prevalent and robust method for post-simulation binding free energy estimation since it takes into account protein flexibility, polarizability, solvation, and entropy, which are often overlooked in docking protocols, and is thus more reliable than most scoring functions used in molecular docking (Ahmad et al., 2022). Therefore, the binding free energy was computed from the trajectory of MD simulation using the MMGB-SA technique to investigate the affinity of STOCK1N-37454 and STOCK3S-30866 towards the 7LWD, 5I73, and 3GWV respectively. A higher affinity for the protein target translates into higher negative binding energy. The average, minimum, and maximum binding energies were computed, and the results are shown in Table 2. Additionally, Tables S2–S13 (Supplementary information) includes the results of computations for several additional interactions, including electrostatic energy, Van der Waals interactions, nonpolar solvation energy, etc. Compounds STOCK1N-37454 and STOCK3S-30866 in complex with 7LWD, 5I73 (central and allosteric), and 3GWV proteins, the estimated average binding energies (ΔG Bind) were recorded as −65.66, −71.25, −68.46, −75.32 and −92.96, −107.39, −96.14, −81.03 kcal/mol, respectively. It is interesting to note that the compound STOCK3S-30866 had the highest negative binding free energy and a docking score that was comparable to its affinity for the evaluated receptors. Additionally, STOCK3S-30866 has higher binding-free energy than the standard drugs Vilazodone, Escitalopram, and Fluoxetine, demonstrating its inhibitory potential. The overall binding energy was found to be negatively impacted by solvation energy (ΔGBindsol GB) and favourably impacted by coulomb (electrostatic) van der Waals energy (ΔGBind vdw).

Principal component analysis

For predicting the dynamic behaviour of a protein, the command line was used in association with the essential dynamics (ED) analysis script (*trj essential dynamics.py*). of the Desmond programme. The main components of the Cα atoms in the protein are calculated by this script. To investigate the protein's conformational distribution over time and the large-scale collective movements of the protein in the protein-ligand complex, PCA was carried out on the MD simulation-generated trajectories. It is possible to identify the major motions within the trajectory as well as the critical

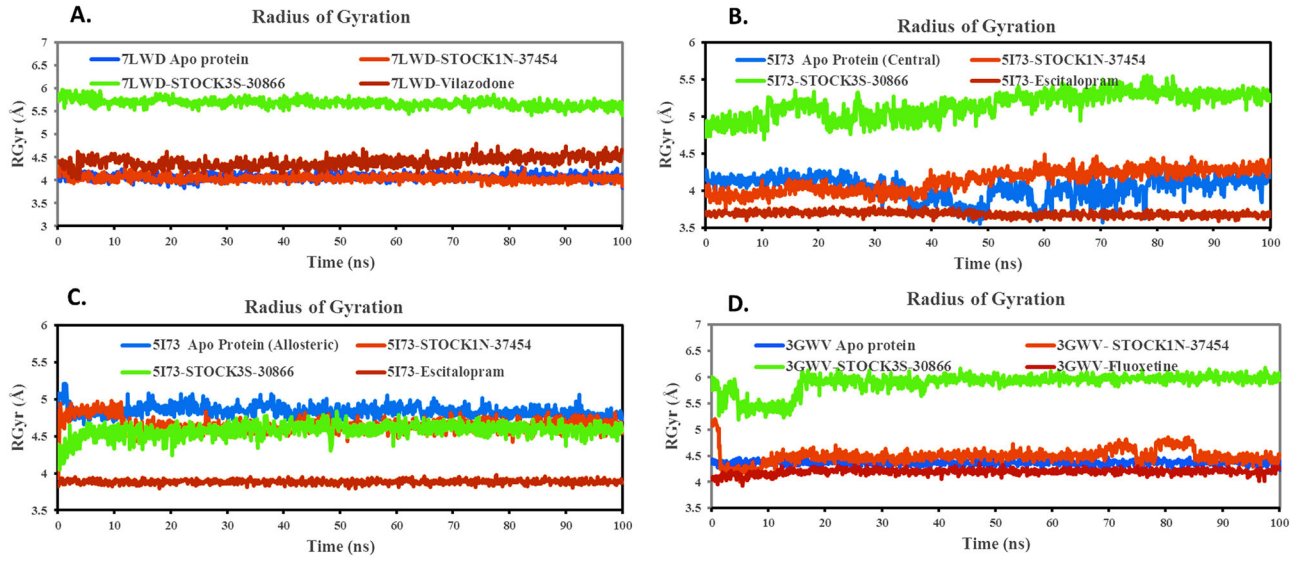


Figure 11. Time-dependent radius of gyration of Apo protein and in complex with STOCK1N-37454, STOCK3S-30866 and standard drug ((a) 7LWD, (b) 5I73 (central), (c) 5I73 (allosteric) and (d) 3GWV) data obtained from MD simulation trajectories.

motions required for conformational changes. Two distinct clusters along the PC1 and PC2 planes are observed in 7LWD bound to STOCK1N-37454 and STOCK3S-30866, non-periodic conformational shift is observed where the trajectories' centering is small away from Apo protein and the standard drug 7LWD-Vilazodone complex. Projection of the motion for the protein in phase space along the PC1 and PC2 for 5I73 (central), 5I73 (allosteric) and 3GWV complexes showed uniform distribution of the conformations throughout the simulations. In these complexes, the **global** motion is highly periodic because the groupings along the PC1 and PC2 planes do not completely cluster separately (Figure 12). The trajectories' centering inside a single cluster suggests that MD trajectories move periodically as a result of steady conformational global motion.

Secondary structure analysis

Furthermore, secondary structure analyses were conducted to assess the changes in the secondary structures induced by the binding of the representative compounds. The percentage of secondary structure content in a protein is an important metric in the study of structural behaviour change. Protein secondary structure elements (SSE) like α-helices and β-strands are monitored throughout the simulation and represented in blue and orange colours, respectively, as shown in Figures S5–S6. In this study, we monitored the changes in SSE, which provides detailed information about the loss and gain of the secondary structure all through the simulation of 7LWD, central 5I73, allosteric 5I73, and 3GWV proteins due to the binding of STOCK1N-37454 and STOCK3S-30866 during the simulation. The participation percentages of helix, strand, and total SSE of Apo protein and ligand-protein complexes are detailed (Supplementary file, Figures S5–S6). In SSE analysis, the most significant structural change was an increase in helical content, which was observed in all studied complexes. Except for the STOCK1N-37454 complex, all residues in Apo protein and the complex with STOCK3S-30866 stably maintained the secondary structure content of 7LWD protein. The residues 475–490 displayed a variation of conformations throughout the simulation in the STOCK1N–37454 complex, where the helix disappears under dynamic conditions. According to the result in Table 2, the binding of STOCK1N-37454 and STOCK3S-30866 to the assessed proteins did not significantly alter their secondary structure.

Physicochemical, pharmacokinetics, pharmacodynamics and toxicity predictions

An effective drug candidate must have a balance of potency, pharmacokinetics, and toxicity such that it is delivered and eliminated from the target without potentiating acute toxicity (Pires et al., 2015). The pk-CSM platform had been verified for its quality and precision (Pires et al., 2015); consequently, it was utilised to predict the drug-likeness and physicochemical properties of compounds of interest. Furthermore, a low-cost and time-saving computational strategy frequently outperforms and is preferred by the researcher over a costly and time-consuming experimental examination. The projected physicochemical and ADMET parameters of four selected ligands, as well as the reference drugs (fluoxetine and vilazodone), are shown in Table 3. Lipinski and his colleagues stated that the following RO5 criteria must not be violated more than once for a drug to be classified as orally active: MW $\leq$ 500 Da, HBD $\leq$ 5, HBA $\leq$ 10, log P $\leq$ 5 and RB $\leq$ 10 (Lipinski et al., 2001; NaAllah et al., 2020). The analysis confirmed that all compounds meet Lipinski's RO5. The log P value of **STOCK3S-30866** (5.66408) is marginally above the threshold, indicating increased lipophilicity and preferential solubility in octanol over water. Compounds with log P values ranging from 1 to 4 are more likely to have ideal qualities as an orally administered medication (Gao et al., 2017). Thus, **STOCK1N-37454** with a higher log P value (3.4364) than reference drugs, reflecting a better lipophilicity profile. Next, the TPSA value reflects intestinal absorption and permeability of BBB (Shayan et al.,

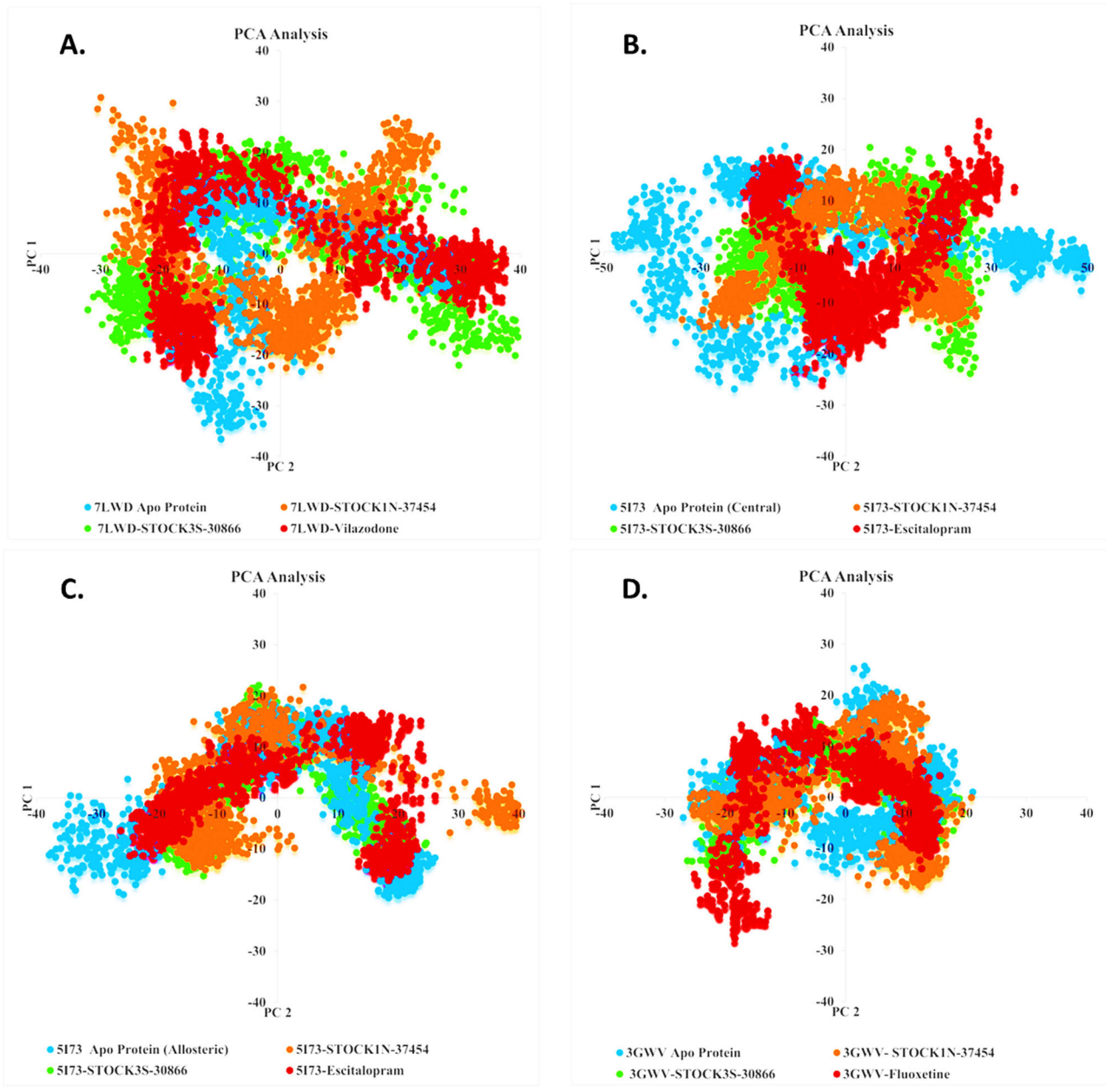


Figure 12. Projection of the motion for Cα atoms Apo protein and in complex with STOCK1N-37454, STOCK3S-30866 and standard drug ((a) 7LWD, (b) 5I73 (central), (c)5I73 (allosteric) and (d) 3GWV) data from obtained MD simulation trajectories.

2021). Although all compounds investigated had high TPSA values ranging from 176.397 to 211.3292 Å^2, they did not differ much from **vilazodone**, which had a TPSA value of 191.9132 Å^2. This is why TPSA value should not be the absolute criteria to rule out these drug candidates as intestinal absorption and BBB penetrance were not solely associated with TPSA.

Interestingly, **STOCK1N-37454** had a better-predicted water solubility profile as compared to **fluoxetine**. In addition to that, all compounds of interest displayed superior skin permeability and gastrointestinal absorption. With these skin permeability features, it may be conceivable to use methods other than oral administration, such as transdermal delivery systems that provide continuous release of drug formulations (Tijani et al., 2021). If only absorption criteria were considered, the compound with the most beneficial properties would be **STOCK1N-37454**, which has nearly identical key characteristics to **vilazodone**. When compared to other ligands and reference drugs, **STOCK1N-37454** was shown to have a more favourable distribution profile, specifically because it is more likely to be in a bound-free state in plasma. The fraction unbound is a strong factor of therapeutic efficacy since only the free form of the drug in plasma may exert pharmacological action via interaction with pharmacological target proteins (Watanabe et al., 2018). Active CNS compounds generally have high BBB and CNS permeability, which is crucial for their involvement in modulating neuronal function (Han, 2021). In light of this, these features are present in all of the studied compounds, which show a high potential for BBB and CNS crossing.

For metabolism parameters, these compounds are predicted to be metabolized by the two most prominent cytochrome

Table 3. Predicted physicochemical, pharmacokinetics, pharmacodynamics and toxicity profiles of selected ligands and references.

Properties	Descriptors	STOCK3S-30866	STOCK1N-37454	STOCK1N-40491	STOCK2S-81285	Fluoxetine	Vilazodone
MW	(g/mol)	498.583	413.521	482.411	404.51	309.331	441.535
Log P	–	5.66408	3.4364	4.7432	4.0049	4.435	4.02958
#Rot. bonds	–	6	4	4	9	6	7
#HBA	–	5	5	5	5	2	5
#HBD	–	2	1	1	2	1	2
TPSA	$(Å)^2$	211.329	180.689	201.296	176.397	127.473	191.913
Absorption	Water solubility (log mol/L)	−6.077	−3.945	−4.172	−5.129	−4.455	−3.898
Absorption	Caco2 permeability	0.572	0.635	0.937	0.773	1.764	1
Absorption	Intestinal absorption (%) (human)	91.658	93.093	94.13	90.433	91.371	92.768
Absorption	Skin permeability (log Kp)	−2.738	−2.768	−2.778	−2.735	−2.482	−2.759
Absorption	P-glycoprotein substrate	Yes	Yes	Yes	Yes	No	Yes
Absorption	P-glycoprotein I inhibitor	Yes	Yes	Yes	Yes	Yes	Yes
Absorption	P-glycoprotein II inhibitor	Yes	Yes	Yes	Yes	No	Yes
Distribution	VDss (human)	−0.115	1.354	1.583	0.395	1.19	0.84
Distribution	Fraction unbound (human)	0.006	0.184	0.102	0.03	0.037	0.067
Distribution	BBB permeability	−0.312	0.289	0.428	0.172	0.501	−0.616
Distribution	CNS permeability	−1.876	−2.052	−1.791	−2.333	−1.329	−2.146
Metabolism	CYP2D6 substrate	No	Yes	Yes	Yes	No	Yes
Metabolism	CYP3A4 substrate	Yes	Yes	Yes	Yes	Yes	Yes
Metabolism	CYP1A2 inhibitor	No	Yes	Yes	Yes	Yes	Yes
Metabolism	CYP2C19 inhibitor	Yes	No	Yes	No	Yes	Yes
Metabolism	CYP2C9 inhibitor	Yes	No	No	No	No	Yes
Metabolism	CYP2D6 inhibitor	No	Yes	Yes	Yes	Yes	No
Metabolism	CYP3A4 inhibitor	Yes	Yes	Yes	Yes	No	Yes
Excretion	Total clearance (log mL/min/kg)	0.072	0.872	0.793	1.287	0.694	1.206
Excretion	Renal OCT2 substrate	No	No	No	No	Yes	No
Toxicity	AMES toxicity	No	No	No	Yes	No	Yes
Toxicity	Max. tolerated dose (log mg/kg/day)	0.276	0.311	0.025	0.241	0.535	0.014
Toxicity	hERG I inhibitor	No	No	No	No	No	No
Toxicity	hERG II inhibitor	Yes	Yes	Yes	Yes	Yes	Yes
Toxicity	Oral Rat acute toxicity (LD50) (mol/kg)	1.855	2.724	2.681	1.946	2.877	2.434
Toxicity	Oral Rat chronic toxicity (LOAEL) (log mg/kg/day)	0.805	1.425	1.373	0.906	1.093	1.568
Toxicity	Hepatotoxicity	Yes	Yes	Yes	Yes	Yes	Yes
Toxicity	Skin sensitisation	No	No	No	No	No	No
Toxicity	*T. Pyriformis* toxicity (log μg/L)	0.291	0.295	0.3	0.308	2.119	0.355
Toxicity	Minnow toxicity (log mM)	−0.631	−0.217	−0.818	0.228	1.25	0.768

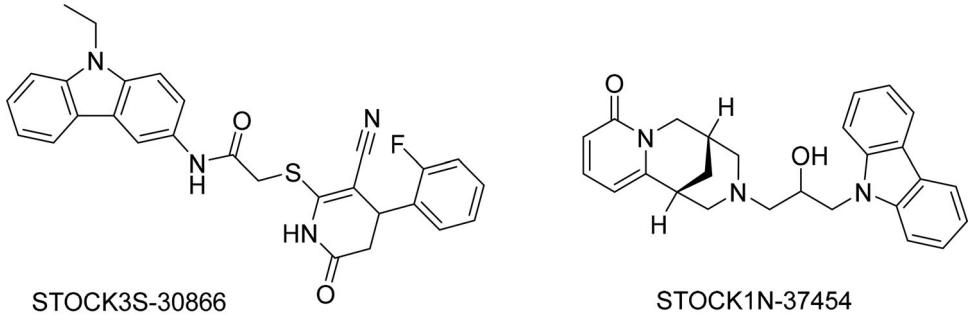


Figure 13. Chemical structures of the IBScreen database carbazole derivatives with potentials for network competitive and allosteric interactions with SERTs as promising antidepressants.

P450 (CYP) enzyme isoforms for drug metabolism, 2D6 and 3A4 (Pires et al., 2015). Despite this, they are anticipated to have multiple CYP enzyme isoforms inhibitory potentials, such as CYP1A2, 2C19, 2C9, 2D6, and 3A4. Yet, when compared to **vilazodone**, **STOCK3S-30866**, **STOCK1N-37454**, and **STOCK2S-31285** target fewer CYP enzymes. With a careful assessment of inhibitory potential, pharmacokinetic drug-drug interactions (DDIs) that result in undesirable adverse effects can be avoided (Lynch & Price, 2007). Further, because **STOCK3S-30866**, **STOCK1N-37454**, and **STOCK1N-40491** displayed negative AMES toxicity, these chemical compounds have no mutagenic potential. All of them, including the reference drugs, are not hERG I inhibitors but inhibit hERG II, implying that they may cause potentially fatal ventricular arrhythmias (Calderone et al., 2010), although, this requires experimental validation. They were predicted not to cause skin sensitization, highlighting the potential application of transdermal delivery. Unfortunately, all, including **fluoxetine** and **vilazodone** show signals for drug-induced liver injury, which must be considered in future clinical research. Surprisingly, *T. pyriformis* toxicity prediction for compounds of interest was lower in comparison to reference drugs. The general ADMET properties of the majority of compounds, especially **STOCK1N-37454**, are comparable to those of **fluoxetine** and **vilazodone**, lending credit to the notion that they are promising druggable candidates. The rest of them can also go through the lead optimization phase, which is frequently used to improve absorption and lower hERG liability (Hughes et al., 2011). The chemical structures of the finally identified ligands support promising multi-dimensional polypharmacological antidepressant potentials with SERTs. These are indicated

by the presence of some relevant pharmacophores in their molecular structures (Figure 13). These include aromatic and amine groups consistently with all reference drugs, fluoro-substituted benzene groups similar to (S)-citalopram, cyano group commonly to (S)-citalopram and vilazodone. Interestingly, the selected compounds are commercially available and have good synthetic accessibility for further studies.

Conclusion

Despite the alarming burden of depression globally, most of the currently available antidepressants remain challenged with several limitations including low efficacy, treatment-resistance, delayed actions and unbearable side effects. Whereas, drug candidates with a propensity for polypharmacology have become more attractive for enhanced efficacy and minimal aftereffects. Relevantly, some candidates such as vilazodone and (S)-citalopram have been shown to demonstrate these advantages. However, they oftentimes also require adjuvant treatment for effectiveness, thus, searching for improved candidates remains crucial. In this study, a computational approach has been employed to identify promising ligands of carbazole scaffold from chemical libraries. The finally selected ligands, **STOCK3S-30866** and **STOCK1N-37454** were demonstrated with more potent binding interactions with hSERTs in comparison with some renowned antidepressants, fluoxetine, vilazodone and *(S)*-citalopram. Their interactions and conformational stabilities in complexes with the selected receptors support the potential for network pharmacological expressions along the serotonergic pathways amenable to the effective treatment of MDD. These include competitive and allosteric inhibition on SERT to potently inhibit the 5-HT reuptake in the synapse, typical of vilazodone and *(S)*-citalopram, and SSR inhibition on SERT to effectively suppress synaptic 5-HT reuptake typical of fluoxetine. The molecular modelling applications herein applied standard theoretical simulations of the drug-like potentials of the selected compounds against the targets. Although, experimental validations are critically required to establish the potentials recorded for the ligands more confidently. However, the study demonstrates an environmentally friendly, economical and speedy screening of lead-like candidates as an early phase of drug discovery for rigorous experimental studies.

Disclosure statement

The authors declare no conflict of interest.

Funding

This work was financially supported by the Tertiary Education Fund Nigeria, Fundamental Research Grant Scheme, Ministry of Higher Education of Malaysia (grant no. 203.CDADAH.6711955). YOA is thankful to the Universiti Sains Malaysia for GA Scheme (grant no. 308.AIPS.415401).

ORCID

Iqrar Ahmad http://orcid.org/0000-0002-7697-9572
Chien Fung Chong http://orcid.org/0000-0002-5149-9433

Author contributions

The manuscript was written with the contributions of all authors. All authors have approved the final version of the manuscript. Conceptualization, literature survey, data collection and writing by YOA, data collection and writing by AI, HP, CFC, NAZ and SYN, visualization, research supervision and manuscript revision by MNM.

References

ADAA. (2021). Understanding anxiety and depression. Anxiety & Depression Association of America. https://adaa.org/understanding-anxiety/depression

Ahmad, I., Akand, S. R., Shaikh, M., Pawara, R., Manjula, S. N., & Patel, H. (2022). Synthesis, molecular modelling study of the methaqualone analogues as anti-convulsant agent with improved cognition activity and minimized neurotoxicity. *Journal of Molecular Structure*, *1251*, 131972. https://doi.org/10.1016/j.molstruc.2021.131972

Ahmad, I., Pawara, R. H., Girase, R. T., Pathan, A. Y., Jagatap, V. R., Desai, N., Ayipo, Y. O., Surana, S. J., & Patel, H. (2022). Synthesis, molecular modeling study, and quantum-chemical-based investigations of isoindoline-1,3-diones as antimycobacterial agents. *ACS Omega*, *7*(25), 21820–21844. https://doi.org/10.1021/ACSOMEGA.2C01981/SUPPL_FILE/AO2C01981_SI_001.PDF

Alapi, E. M., & Fischer, J. (2006). Table of selected analogue classes. In *Analogue-based drug discovery* (pp. 441-552). Weinheim: WILEY-VCH Verlag GmbH & Co. KGaA. https://doi.org/10.1002/3527608001.ch23

Allais, G., & Benedetto, C. (2016). Spotlight on frovatriptan: A review of its efficacy in the treatment of migraine. *Drug Design, Development and Therapy*, *10*, 3225–3236. https://doi.org/10.2147/DDDT.S105932

Ayipo, Y. O., Yahaya, S. N., Babamale, H. F., Ahmad, I., Patel, H., & Mordi, M. N. (2021). β-Carboline alkaloids induce structural plasticity and inhibition of SARS-CoV-2 nsp3 macrodomain more potently than remdesivir metabolite GS-441524: Computational approach. *Turkish Journal of Biology*, *45*(SI-1), 503–517. https://doi.org/10.3906/biy-2106-64

Ayipo, Y. O., Alananzeh, W. A., Yahaya, S. N., & Mordi, M. N. (2022). Molecular modelling and virtual screening to identify new piperazine derivatives as potent human 5-HT1A antagonists and reuptake inhibitors. *Combinatorial Chemistry & High Throughput Screening*, *25*, 1–20. https://doi.org/10.2174/1386207325666220524094913

Ayipo, Y. O., Alananzeh, W. A., Ahmad, I., Patel, H., & Mordi, M. N. (2022). Structural modelling and in silico pharmacology of β-carboline alkaloids as potent 5-HT1A receptor antagonists and reuptake inhibitors. *Journal of Biomolecular Structure and Dynamics*, *0*(0), 1–17. https://doi.org/10.1080/07391102.2022.2104376

Bauman, M. D., Schumann, C. M., Carlson, E. L., Taylor, S. L., Vázquez-Rosa, E., Cintrón-Pérez, C. J., Shin, M. K., Williams, N. S., & Pieper, A. A. (2018). Neuroprotective efficacy of P7C3 compounds in primate hippocampus. *Translational Psychiatry*, *8*(1), 1–11. https://doi.org/10.1038/s41398-018-0244-1

Berger, N. D., Gadotti, V. M., Petrov, R. R., Chapman, K., Diaz, P., & Zamponi, G. W. (2014). NMP-7 inhibits chronic inflammatory and neuropathic pain via block of Cav3.2T-type calcium channels and activation of CB2 receptors. *Molecular Pain*, *10*(1), 77. https://doi.org/10.1186/1744-8069-10-77

Berger, S. I., & Iyengar, R. (2009). Network analyses in systems pharmacology. *Bioinformatics (Oxford, England)*, *25*(19), 2466–2472. https://doi.org/10.1093/bioinformatics/btp465

Branco, J. C., Tomé, A. M., Cruz, M. R., & Filipe, A. (2011). Pirlindole in the treatment of depression and fibromyalgia syndrome. *Clinical Drug Investigation*, *31*(10), 675–689. https://doi.org/10.2165/11595410-000000000-00000

Brigitta, B. (2002). Pathophysiology of depression and mechanisms of treatment. *Dialogues in Clinical Neuroscience*, *4*(1), 7–20. https://doi.org/10.31887/dcns.2002.4.1/bbondy

Brody, T. (2018). Food effect studies. In *FDA's drug review process and the package label* (pp. 35-100). Elsevier Inc. https://doi.org/10.1016/b978-0-12-814647-7.00003-8

Calderone, V., Testai, L., Martinotti, E., Del Tacca, M., & Breschi, M. C. (2010). Drug-induced block of cardiac HERG potassium channels and development of torsade de pointes arrhythmias: The case of antipsychotics. *Journal of Pharmacy and Pharmacology*, *57*(2), 151–161. https://doi.org/10.1211/0022357055272

Castro-Alvarez, A., Costa, A. M., & Vilarrasa, J. (2017). The performance of several docking programs at reproducing protein-macrolide-like crystal structures. *Molecules*, *22*(1), 1-14. https://doi.org/10.3390/molecules22010136

Chaudhari, B., Patel, H., Thakar, S., Ahmad, I., & Bansode, D. (2022). Optimizing the sunitinib for cardio-toxicity and thyro-toxicity by scaffold hopping approach. *In Silico Pharmacology*, *10*(1), 10. https://doi.org/10.1007/s40203-022-00125-1

Chilmonczyk, Z., Bojarski, A. J., Pilc, A., & Sylte, I. (2017). Serotonin transporter and receptor ligands with antidepressant activity as neuroprotective and proapoptotic agents. *Pharmacological Reports: PR*, *69*(3), 469–478. https://doi.org/10.1016/j.pharep.2017.01.011

Coleman, J. A., Green, E. M., & Gouaux, E. (2016). X-ray structures and mechanism of the human serotonin transporter. *Nature*, *532*(7599), 334–339. https://doi.org/10.1038/nature17629

Cowen, P. J., & Browning, M. (2015). What has serotonin to do with depression?. *World Psychiatry: Official Journal of the World Psychiatric Association (WPA)*, *14*(2), 158–160. https://doi.org/10.1002/wps.20229

D. E. Shaw Research & Schrödinger Release. (2021). Desmond molecular dynamics system. Maestro-Desmond interoperability tools. In DE Shaw Research.

de Sousa, D. P., Schefer, R. R., Brocksom, U., & Brocksom, T. J. (2006). Synthesis and antidepressant evaluation of three para-benzoquinone mono-oximes and their oxy derivatives. *Molecules (Basel, Switzerland)*, *11*(2), 148–155. https://doi.org/10.3390/11020148

Deodhar, M., Al Rihani, S. B., Arwood, M. J., Darakjian, L., Dow, P., Turgeon, J., & Michaud, V. (2020). Mechanisms of CYP450 Inhibition: Understanding drug-drug interactions due to mechanism-based inhibition in clinical practice. *Pharmaceutics*, *12*(9), 1–18. https://doi.org/10.3390/PHARMACEUTICS12090846

Fronza, M. G., Pinto Brod, L. M., Casaril, A. M., Sacramento, M., Alves, D., & Savegnago, L. (2017). Computational and biological evidences on the serotonergic involvement of SeTACN antidepressant-like effect in mice. *Plos One*, *12*(11), e0187445. https://doi.org/10.1371/journal.pone.0187445

Gangadharan, N. T., Venkatachalam, A. B., & Sugathan, S. (2017). High-throughput and in silico screening in drug discovery. *Bioresources and Bioprocess in Biotechnology*, *1*, 247–273. https://doi.org/10.1007/978-981-10-3573-9

Gao, Y., Gesenberg, C., & Zheng, W. (2017). Oral formulations for preclinical studies: Principle, design, and development considerations. *Developing Solid Oral Dosage Forms: Pharmaceutical Theory and Practice: Second Edition*, ch 17, 455–495. Elsevier Inc. https://doi.org/10.1016/B978-0-12-802447-8.00017-0

Guedes, I. A., de Magalhães, C. S., & Dardenne, L. E. (2014). Receptor-ligand molecular docking. *Biophysical Reviews*, *6*(1), 75–87. https://doi.org/10.1007/s12551-013-0130-2

Han, L. (2021). Modulation of the blood–brain barrier for drug delivery to brain. *Pharmaceutics*, *13*(12), 1-19. https://doi.org/10.3390/PHARMACEUTICS13122024

Harder, E., Damm, W., Maple, J., Wu, C., Reboul, M., Xiang, J. Y., Wang, L., Lupyan, D., Dahlgren, M. K., Knight, J. L., Kaus, J. W., Cerutti, D. S., Krilov, G., Jorgensen, W. L., Abel, R., & Friesner, R. A. (2016). OPLS3: A force field providing broad coverage of drug-like small molecules and proteins. *Journal of Chemical Theory and Computation*, *12*(1), 281–296. https://doi.org/10.1021/acs.jctc.5b00864

Hart, L. R., Lebedenko, C. G., Mitchell, S. M., Daso, R. E., & Banerjee, I. A. (2022). In silico studies of tumor targeted peptide-conjugated natural products for targeting over-expressed receptors in breast cancer cells using molecular docking, molecular dynamics and MMGBSA calculations. *Applied Sciences (Switzerland)*, *12*(1), 515. https://doi.org/10.3390/APP12010515/S1

Hegden, P. R., Emmanuel, B. D., Beevi, J., & Dharan, S. S. (2020). A concise review on carbazole derivatives and its biological activities. *Journal of Pharmaceutical Sciences and Research*, *12*(10), 1271–1277.

Holshoe, J. M. (2016). Antidepressants and sleep. *The Curated Reference Collection in Neuroscience and Biobehavioral Psychology, August 2015*, 617–620. Elsevier Inc. https://doi.org/10.1016/B978-0-12-809324-5.00973-1

Hughes, J. P., Rees, S. S., Kalindjian, S. B., & Philpott, K. L. (2011). Principles of early drug discovery. *British Journal of Pharmacology*, *162*(6), 1239–1249. https://doi.org/10.1111/j.1476-5381.2010.01127.x

Huskisson, E. C. (1982). Carprofen. *European Journal of Rheumatology and Inflammation*, *5*(4), 333–334. https://doi.org/10.2165/00128415-200812030-00045

Immadisetty, K. (2015). *Modeling the binding of inhibitors/drugs to the human serotonin transporter* [Doctoral dissertation]. Duquesne University.

Ivanova, L., Tammiku-Taul, J., García-Sosa, A. T., Sidorova, Y., Saarma, M., & Karelson, M. (2018). Molecular dynamics simulations of the interactions between glial cell line-derived neurotrophic factor family receptor GFRα1 and small-molecule ligands. *ACS Omega*, *3*(9), 11407–11414. https://doi.org/10.1021/ACSOMEGA.8B01524/ASSET/IMAGES/LARGE/AO-2018-01524B_0008.JPEG

Jean, B. (2017). *Modeling the binding of neurotransmitter transporter inhibitors with molecular dynamics and free energy calculations* [Doctoral dissertation]. Duquesne University. https://dsc.duq.edu/etd/240

Lexow, M., Wernecke, K., Schmid, G. L., Sultzer, R., Bertsche, T., & Schiek, S. (2021). Considering additive effects of polypharmacy: Analysis of adverse events in geriatric patients in long-term care facilities. *Wiener Klinische Wochenschrift*, *133*(15–16), 816–824. https://doi.org/10.1007/s00508-020-01750-6

Lipinski, C. A., Lombardo, F., Dominy, B. W., & Feeney, P. J. (2001). Experimental and computational approaches to estimate solubility and permeability in drug discovery and development q settings. *Advanced Drug Delivery Reviews*, *46*(1–3), 3–26. https://doi.org/10.1016/s0169-409x(00)00129-0

Lynch, T., & Price, A. (2007). The effect of cytochrome P450 metabolism on drug response, interactions, and adverse effects. *American Family Physician*, *76*(3), 391–6.

Madhavi Sastry, G., Adzhigirey, M., Day, T., Annabhimoju, R., & Sherman, W. (2013). Protein and ligand preparation: Parameters, protocols, and influence on virtual screening enrichments. *Journal of Computer-Aided Molecular Design*, *27*(3), 221–234. https://doi.org/10.1007/s10822-013-9644-8

Moreira, L. K. D. S., Silva, R. R., Silva, D. M., Mendes, M. A. S., de Brito, A. F., de Carvalho, F. S., Sanz, G., Rodrigues, M. F., da Silva, A. C. G., Thomaz, D. V., de Oliveira, V., Vaz, G. B., Lião, M. L., Valadares, M. C., Gil, E. D. S., Costa, E. A., Noël, F., & Menegatti, R. (2022). Anxiolytic- and antidepressant-like effects of new phenylpiperazine derivative LQFM005 and its hydroxylated metabolite in mice. *Behavioural Brain Research*, *417*(1), 113582. https://doi.org/10.1016/j.bbr.2021.113582

NaAllah, A., Ayipo, Y. O., Komolafe, D. I., Solihu, S., Bamidele, B., Alabi, M. A., Balogun, A.-A., Abdulazeez, A. T., & Mordi, M. N. (2021). Phytochemical screening and in silico pharmacological profiling of ethanolic extract of Aframomum melegueta for prostate carcinoma. *Journal of Applied Pharmaceutical Science*, *11*(7), 132-145. https://doi.org/10.7324/JAPS.2021.110715

Navratna, V., Tosh, D. K., Jacobson, K. A., & Gouaux, E. (2018). Thermostabilization and purification of the human dopamine transporter (hDAT) in an inhibitor and allosteric ligand bound conformation. *Plos One*, *13*(7), e0200085. https://doi.org/10.1371/journal.pone.0200085

Obaidullah, A. J., Alanazi, M. M., Alsaif, N. A., Alanazi, A. S., Albassam, H., Az, A., Alwassil, O. I., Alqahtani, A., M., & Tareq, A. M. (2022). Network pharmacology- and molecular docking-based identification of potential phytocompounds from Argyreia capitiformis in the treatment of inflammation. *Evidence-Based Complementary and Alternative Medicine: eCAM*, *2022*, 8037488. https://doi.org/10.1155/2022/8037488

Park, Y. S., & Sung, K. W. (2019). Selective serotonin reuptake inhibitor escitalopram inhibits 5-HT3 receptor currents in NCB-20 cells. *The Korean Journal of Physiology & Pharmacology: Official Journal of the Korean Physiological Society and the Korean Society of Pharmacology*, *23*(6), 509–517. https://doi.org/10.4196/kjpp.2019.23.6.509

Peng, J., Zhang, K., Wang, L., Peng, F., Zhang, C., Long, K., Chen, J., Zhou, X., Gao, P., & Fan, G. (2022). Integrating network pharmacology and molecular docking to explore the potential mechanism of Xinguan No. 3 in the treatment of COVID-19. *Open Chemistry*, *20*(1), 570–582. https://doi.org/10.1515/chem-2022-0178

Peng, Y., McCorvy, J. D., Harpsøe, K., Lansu, K., Yuan, S., Popov, P., Qu, L., Pu, M., Che, T., Nikolajsen, L. F., Huang, X.-P., Wu, Y., Shen, L., Bjørn-Yoshimoto, W. E., Ding, K., Wacker, D., Han, G. W., Cheng, J., Katritch, V., … Liu, Z.-J. (2018). 5-HT2C Receptor structures reveal the structural basis of GPCR polypharmacology. *Cell*, *172*(4), 719–730.e14. https://doi.org/10.1016/j.cell.2018.01.001

Peng, Y., Zhao, S., Wu, Y., Cao, H., Xu, Y., Liu, X., Shui, W., Cheng, J., Zhao, S., Shen, L., Ma, J., Quinn, R. J., Stevens, R. C., Zhong, G., & Liu, Z.-J. (2018). Identification of natural products as novel ligands for the human 5-HT2C receptor. *Biophysics Reports*, *4*(1), 50–61. https://doi.org/10.1007/s41048-018-0047-1

Pires, D. E. V., Blundell, T. L., & Ascher, D. B. (2015). pkCSM: Predicting small-molecule pharmacokinetic and toxicity properties using graph-based signatures. *Journal of Medicinal Chemistry*, *58*(9), 4066–4072. https://doi.org/10.1021/acs.jmedchem.5b00104

Plenge, P., Abramyan, A. M., Sørensen, G., Mørk, A., Weikop, P., Gether, U., Bang-Andersen, B., Shi, L., & Loland, C. J. (2020). The mechanism of a high-affinity allosteric inhibitor of the serotonin transporter. *Nature Communications*, *11*(1), 1–12. https://doi.org/10.1038/s41467-020-15292-y

Plenge, P., Yang, D., Salomon, K., Laursen, L., Kalenderoglou, I. E., Newman, A. H., Gouaux, E., Coleman, J. A., & Loland, C. J. (2021). The antidepressant drug vilazodone is an allosteric inhibitor of the serotonin transporter. *Nature Communications*, *12*(1), 1-12. https://doi.org/10.1038/s41467-021-25363-3

Potamitis, C., Siakouli, D., Papavasileiou, K. D., Boulaka, A., Ganou, V., Roussaki, M., Calogeropoulou, T., Zoumpoulakis, P., Alexis, M. N., Zervou, M., & Mitsiou, D. J. (2019). Discovery of new non-steroidal selective glucocorticoid receptor agonists. *The Journal of Steroid Biochemistry and Molecular Biology*, *186*, 142–153. https://doi.org/10.1016/j.jsbmb.2018.10.007

Prieto-Martínez, F. D., López-López, E., Eurídice Juárez-Mercado, K., & Medina-Franco, J. L. (2019). Computational drug design methods—current and future perspectives. *In Silico Drug Design*, *3*, 19–44. https://doi.org/10.1016/b978-0-12-816125-8.00002-x

Que, W., Chen, M., Yang, L., Zhang, B., Zhao, Z., Liu, M., Cheng, Y., & Qiu, H. (2021). A network pharmacology-based investigation on the bioactive ingredients and molecular mechanisms of Gelsemium elegans Benth against colorectal cancer. *BMC Complementary Medicine and Therapies*, *21*(1), 1–18. https://doi.org/10.1186/s12906-021-03273-7

Ragno, R., Esposito, V., Di Mario, M., Masiello, S., Viscovo, M., & Cramer, R. D. (2020). Teaching and learning computational drug design: Student investigations of 3D quantitative structure-activity relationships through web applications. *Journal of Chemical Education*, *97*(7), 1922–1930. https://doi.org/10.1021/acs.jchemed.0c00117

Ramadan, A. M., & Mansour, I. A. (2020). Could ketamine be the answer to treating treatment-resistant major depressive disorder?. *General Psychiatry*, *33*(5), e100227. https://doi.org/10.1136/gpsych-2020-100227

Ramírez, D., & Caballero, J. (2018). Is it reliable to take the molecular docking top scoring position as the best solution without considering available structural data?. *Molecules*, *23*(5), 1–17. https://doi.org/10.3390/molecules23051038

Rudnick, G. (2007). SERT, serotonin transporter. In *xPharm: The comprehensive pharmacology reference* (pp. 1–6). Elsevier Inc. https://doi.org/10.1016/B978-008055232-3.60442-8

Sahli, Z. T., Banerjee, P., & Tarazi, F. I. (2016). The preclinical and clinical effects of vilazodone for the treatment of major depressive disorder. *Expert Opinion on Drug Discovery*, *11*(5), 515–523. https://doi.org/10.1517/17460441.2016.1160051

Samdani, M. N., Morshed, N., Reza, R., Asaduzzaman, M., & Islam, A. B. M. M. K. (2022). Targeting SARS-CoV-2 non-structural protein 13 via helicase-inhibitor-repurposing and non-structural protein 16 through pharmacophore-based screening. *Molecular Diversity*, *12*, 1–19. https://doi.org/10.1007/s11030-022-10468-8

Schaduangrat, N., Lampa, S., Simeon, S., Gleeson, M. P., Spjuth, O., & Nantasenamat, C. (2020). Towards reproducible computational drug discovery. *Journal of Cheminformatics*, *12*(1), 1–30. https://doi.org/10.1186/s13321-020-0408-x

Shadrina, M., Bondarenko, E. A., & Slominsky, P. A. (2018). Genetics factors in major depression disease. *Frontiers in Psychiatry*, *9*(JUL), 334. https://doi.org/10.3389/fpsyt.2018.00334

Shahwar, D., Saeed, M., Hazrat, H., Javaid, S., Mohsin, S., Ul-Haq, Z., & Chotani, M. A. (2022). The nucleoside adenosine inhibits intracellular microvascular α 2C-adrenoceptor surface trafficking. *Journal of Molecular Structure*, *1267*, 133637. https://doi.org/10.1016/j.molstruc.2022.133637

Shayan, S., Jamaran, S., Askandar, R. H., Rahimi, A., Elahi, A., Farshadfar, C., & Ardalan, N. (2021). The SARS-Cov-2 Proliferation blocked by a novel and potent main protease inhibitor via computer-aided drug design. *Iranian Journal of Pharmaceutical Research*, *20*(3), 399-418. https://doi.org/10.22037/IJPR.2021.114846.15061

Sheikh-Taha, M., & Asmar, M. (2021). Polypharmacy and severe potential drug-drug interactions among older adults with cardiovascular disease in the United States. *BMC Geriatrics*, *21*(1), 1–6. https://doi.org/10.1186/s12877-021-02183-0

Si, T., & Wang, P. (2014). When is antidepressant polypharmacy appropriate in the treatment of depression?. *Shanghai Archives of Psychiatry*, *26*(6), 357–359. https://doi.org/10.11919/j.issn.1002-0829.214152

Sliwoski, G., Kothiwale, S., Meiler, J., & Lowe, E. W. (2014). Computational methods in drug discovery. *Pharmacological Reviews*, *66*(1), 334–395. https://doi.org/10.1124/pr.112.007336

Smithson, J., & Mitchell, P. B. (2019). Antidepressants. *Side Effects of Drugs Annual*, *41*, 13–26. https://doi.org/10.1016/bs.seda.2019.10.002

Song, S., Zhou, J., Li, Y., Liu, J., Li, J., & Shu, P. (2022). Network pharmacology and experimental verification based research into the effect and mechanism of Aucklandiae Radix–Amomi Fructus against gastric cancer. *Scientific Reports*, *12*(1), 1–30. https://doi.org/10.1038/s41598-022-13223-z

Sorokina, M., & Steinbeck, C. (2020). Review on natural products databases: Where to find data in 2020. *Journal of Cheminformatics*, *12*(1), 20. https://doi.org/10.1186/s13321-020-00424-9

Sundaram, K., Ravi, S., Thenmozhi, M., & Mohanraj, V. (2018). Synthesis, single crystal XRD and molecular docking of 3-α-carboxy ethyl rhodanine. *Asian Journal of Chemistry*, *30*(7), 1446–1450. https://doi.org/10.14233/ajchem.2018.21161

Tijani, A. O., Nunez, E., Singh, K., Khanna, G., & Puri, A. (2021). Transdermal route: A viable option for systemic delivery of antidepressants. *Journal of Pharmaceutical Sciences*, *110*(9), 3129–3149. https://doi.org/10.1016/J.XPHS.2021.05.015

Tomar, V., Mazumder, M., Chandra, R., Yang, J., & Sakharkar, M. K. (2018). Small molecule drug design. *Encyclopedia of Bioinformatics and Computational Biology: ABC of Bioinformatics*, *1–3*, 741–760. https://doi.org/10.1016/B978-0-12-809633-8.20157-X

Vann, M. R. (2021). 12 Surprising Facts About Depression. Everyday Health. https://www.everydayhealth.com/hs/major-depression-health-well-being/surprising-depression-facts/

Wang, G., Han, T., Nijhawan, D., Theodoropoulos, P., Naidoo, J., Yadavalli, S., Mirzaei, H., Pieper, A. A., Ready, J. M., & McKnight, S. L. (2014). P7C3 neuroprotective chemicals function by activating the rate-limiting enzyme in NAD salvage. *Cell*, *158*(6), 1324–1334. https://doi.org/10.1016/j.cell.2014.07.040

Watanabe, R., Esaki, T., Kawashima, H., Natsume-Kitatani, Y., Nagao, C., Ohashi, R., & Mizuguchi, K. (2018). Predicting fraction unbound in human plasma from chemical structure: Improved accuracy in the low value ranges. *Molecular Pharmaceutics*, *15*(11), 5302–5311. https://doi.org/10.1021/ACS.MOLPHARMACEUT.8B00785/ASSET/IMAGES/LARGE/MP-2018-007855_0006.JPEG

Wood, P. L., & McQuade, P. S. (1984). Ciclindole and flucindole: Novel tetrahydrocarbazolamine neuroleptics. *Progress in Neuro-*

Psychopharmacology & Biological Psychiatry, *8*(4–6), 773–777. https://doi.org/10.1016/0278-5846(84)90057-5

Wray, N. H., & Rasenick, M. M. (2019). Lipid rafts in psychiatry. In *Advances in Pharmacology*. (1st ed., Vol. 86). Elsevier Inc. https://doi.org/10.1016/bs.apha.2019.04.001

Yuen, H., Hung, A., Yang, A. W. H., & Lenon, G. B. (2020). Mechanisms of action of cassiae semen for weight management: A computational molecular docking study of serotonin receptor 5-HT2C. *International Journal of Molecular Sciences*, *21*(4), 1326. https://doi.org/10.3390/ijms21041326

Zhou, Z., Zhen, J., Karpowich, N. K., Law, C. J., Reith, M. E. A., & Wang, D. N. (2009). Antidepressant specificity of serotonin transporter suggested by three LeuT-SSRI structures. *Nature Structural & Molecular Biology*, *16*(6), 652–657. https://doi.org/10.1038/nsmb.1602